

Neural ODEs for Stiff Systems: Implicit Single-Step Methods

Colby Fronk¹ and Linda Petzold^{2,3}¹*Department of Chemical Engineering; University of California, Santa Barbara; Santa Barbara, CA 93106, USA^a*²*Department of Mechanical Engineering and Computer Science; University of California, Santa Barbara; Santa Barbara, CA 93106, USA*³*Department of Computer Science; University of California, Santa Barbara; Santa Barbara, CA 93106, USA^b*

(Dated: 10 October 2024)

Stiff systems of ordinary differential equations (ODEs) are pervasive in many science and engineering fields, yet standard neural ODE approaches struggle to learn them. This limitation is the main barrier to the widespread adoption of neural ODEs. In this paper, we propose an approach based on single-step implicit schemes to enable neural ODEs to handle stiffness and demonstrate that our implicit neural ODE method can learn stiff dynamics. This work addresses a key limitation in current neural ODE methods, paving the way for their use in a wider range of scientific problems.

Stiff systems of ordinary differential equations (ODEs) describe systems with widely varying time scales, where the fast scales are stable. These systems are common in various scientific and engineering fields, such as chemistry, biology, and physics, where they describe complex phenomena like chemical reactions or biological processes. However, current neural ordinary differential equations (neural ODEs), which are machine learning models that utilize neural networks to approximate the solutions of differential equations from data, encounter difficulties when dealing with stiff ODE systems due to issues with stability. This limitation has been a significant barrier to their broader use in scientific research and engineering applications. To address this, we propose a new method based on single-step implicit schemes, which enables neural ODEs to handle stiffness effectively. Implicit schemes provide a more stable way to learn stiff dynamics, allowing the model to take larger steps than classical explicit methods. Our approach shows that neural ODEs can now learn stiff systems accurately without the usual stability problems. This advancement opens the door for neural ODEs to be applied in more complex and varied scientific problems.

I. INTRODUCTION

Developing a mathematical model is essential for understanding complex processes in chemistry, biology, and engineering. Ordinary differential equation (ODE) models, for example, describe the spread of diseases like flu, measles, and COVID-19 in epidemiology and the dynamics of CD4 T-cells during HIV infection in medicine. Detailed models help to enable the identification of intervention methods, such as drugs for disease prevention. Mechanistic models, based on first principles like conservation laws and force interactions, provide insights into system behavior under different scenarios,

making them preferable over black-box models to scientists and engineers. However, these models require lengthy development cycles, highlighting the need for tools that can accelerate and support model development.

Sparse Identification of Nonlinear Dynamics (SINDy)¹⁻³ is a recent advancement in system identification, using linear regression of time derivatives against candidate terms to identify ODE models. SINDy has successfully recovered ODE systems across various fields, including fluid dynamics⁴, plasma physics⁵, chemical reaction networks^{6,7}, and optical communication⁸. However, it relies on densely sampled training data⁹. In contrast, neural ODEs⁹⁻²⁰ can handle irregular data and do not have strict requirements on sampling rates or data point frequency.

The rise of data from the Internet of Things^{21,22}, robotics for high-throughput experiments^{23,24}, and earth observation satellites²⁵ has necessitated new methods for processing and understanding large datasets. Neural differential equations and physics-informed neural networks (PINNs)²⁶⁻³² offer powerful frameworks for modeling such systems, but their black-box nature limits their interpretability and generalizability.

Symbolic neural networks are emerging as a response to the demand for more interpretable models. Several architectures^{9,33-40} embed mathematical terms within the network, enabling symbolic regression with neural networks to recover equations that are interpretable and usable by scientists^{9,20}. This approach integrates the strengths of both neural differential equations and mechanistic models, potentially transforming model development cycles.

The main bottleneck preventing the widespread adoption of neural ODEs is their difficulty in handling stiffness. Stiff ODEs are equations in which certain components of the solution vary rapidly compared to others, requiring extremely small time steps for explicit methods to maintain stability. These types of equations frequently arise in real-world problems across fields such as physics, biology, and engineering, where processes occur on multiple time scales. Effectively solving stiff ODEs is critical for accurate and efficient modeling of these complex systems. Furthermore, neural ODEs frequently become stiff during training, even when the training data comes from a non-stiff ODE model. This occurs because

^aCorrespond to colbyfronk@ucsb.edu^bCorrespond to petzold@engineering.ucsb.edu

parameter exploration can introduce stiffness, and the highly expressive nature of neural networks often results in very non-linear differential equations. This additional complication can greatly slow down or even halt the training process, necessitating that all neural ODE methods be robust to stiffness, regardless of whether the underlying model itself is inherently stiff.

Several papers have claimed to address the problem of stiffness in neural ODEs, but most do so only partially by employing techniques such as equation scaling or regularization. These approaches aim to reframe the problem, making it more tractable, rather than directly solving the stiffness issue. For example, scaling/reformulating the equations^{41–49} can reduce the stiffness by modifying the system’s dynamics, while regularization techniques^{50–62} can limit the model’s flexibility, indirectly reducing the likelihood of stiffness. Although these methods offer some relief, they do not fundamentally solve the problem of stiffness in neural ODEs. Truly overcoming this bottleneck requires the development of numerical methods specifically designed for neural ODEs that can handle stiffness without requiring modifications to the original equations. This approach targets the core challenge directly, enabling neural ODEs to be more robust, efficient, and applicable to a broader range of real-world problems.

The Discretize-Optimize (Disc-Opt) and Optimize-Discretize (Opt-Disc) methods are two key strategies for optimizing neural ODEs. In Disc-Opt, the ODE is first discretized, and optimization is then applied to the discretized problem, which is straightforward to implement with automatic differentiation tools⁶³. Conversely, Opt-Disc defines a continuous optimization problem and computes gradients in the continuous domain before discretizing, requiring the numerical solution of the adjoint equation⁶⁴. Ref. 53 shows that Disc-Opt often outperforms Opt-Disc, achieving similar or better validation losses at significantly lower computational costs, with an average 20x speedup. This is partly due to the more reliable gradients in Disc-Opt, unaffected by solver accuracy, allowing flexibility based on data noise levels⁶⁵. Given these advantages, we have focused on Disc-Opt in our research to develop new differential ODE solvers capable of handling stiffness efficiently.

In this paper, we focus on training stiff neural ODEs using single-step implicit methods. Given the challenges associated with stiffness in neural ODEs, our aim is to develop robust numerical methods that can handle the stability issues arising during training without modifying the underlying equations. Single-step implicit methods, which compute the next solution value based only on the current state, are a promising starting point for this endeavor. They provide a relatively simple framework for understanding the dynamics of stiff neural ODEs and for implementing backpropagation through the predicted ODE solutions.

We have initially focused on single-step methods due to their simplicity and ease of implementation, leaving the exploration of more complex multistep methods for future research. Multistep methods, while potentially more efficient in some scenarios, rely on accurate information from multiple previous time points. This dependency complicates their

use in neural ODE training, where data can be noisy or incomplete and additional computations are required to initiate the method. By starting with single-step methods, we lay the groundwork for creating a robust and differentiable ODE solver for stiff neural ODEs. This foundational work is crucial for extending these solvers to a wide range of applications, including partial differential equations (PDEs) with stiffness due to diffusion terms, mesh-based simulations with methods like MeshGraphNets⁶⁶, physics-informed neural networks (PINNs), and other emerging frameworks that require differentiable differential equation solvers.

II. METHODS

A. Neural ODEs

Neural Ordinary Differential Equations¹⁰ (neural ODEs) are a type of neural network designed to approximate time-series data, $y(t)$, by modeling it as an ODE system. In many scientific fields, the ODE system we aim to approximate takes the following form:

$$\frac{dy(t)}{dt} = f(t, y(t), \theta), \quad (1)$$

where t represents time, $y(t)$ is a vector of state variables, θ denotes the parameter vector, and f is the function defining the ODE model. Determining the exact system of equations for f is often a challenging and labor-intensive process. Leveraging the universal approximation theorem⁶⁷, we use a neural network (NN) to approximate the function f :

$$\frac{dy(t)}{dt} = f \approx NN(t, y(t), \theta). \quad (2)$$

Neural ODEs can be handled similarly to traditional ODEs. Predictions for time-series data are generated by integrating the neural ODE starting from an initial condition, utilizing a discretization scheme^{68–70}, just as is done for standard ODEs.

Learning Unknown Components in an ODE Model with Neural ODEs

When the underlying equations of a system are entirely unknown, neural ODEs have the capability to learn the complete model:

$$\frac{dy(t)}{dt} = NN(t, y(t), \theta). \quad (3)$$

However, there are cases where some parts of the model, denoted as f_{known} , are known, but not all mechanisms and terms describing the full model are understood. Here, the neural ODE can learn the unknown terms:

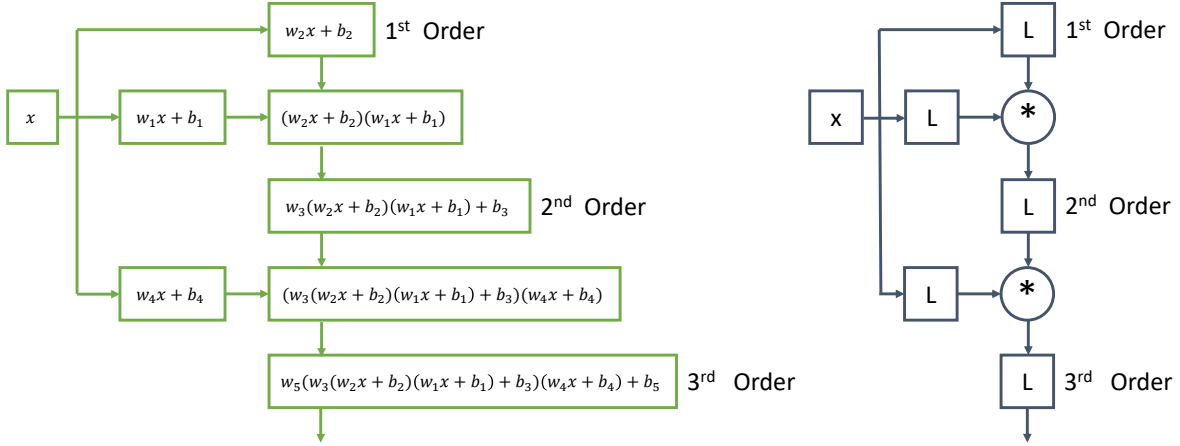


FIG. 1. The architecture of the π -net V1, as described in Ref. 33, is shown on the right. On the left, an example demonstrates how a 1-dimensional input, represented by the variable x , flows through the network. Layers where the Hadamard product is applied to the inputs are indicated by circles marked with a $*$. Standard linear layers, denoted by boxes labeled L , do not employ activation functions. Notably, this design avoids common activation functions such as \tanh or ReLU , enhancing its interpretability.

$$\frac{dy(t)}{dt} = f_{\text{known}}(t, y(t), \theta) + NN(t, y(t), \theta). \quad (4)$$

Learning these missing components does not require extensive special handling; it simply involves incorporating the known terms during the training process.

Polynomial Neural ODEs

Systems in various domains are often modeled by differential equations where the right-hand side functions f are polynomials. Examples include chemical kinetics⁷¹, cell signaling networks⁷² and gene regulatory networks⁷³ in systems biology, as well as population dynamics in epidemiology⁷⁴ and ecology⁷⁵. Polynomial neural ODEs are particularly suitable for this category of inverse problems, where it is known in advance that the system is governed by polynomial expressions.

Polynomial neural networks^{33,76} are a type of neural network architecture where the output is a polynomial function of the input layer. These networks fall under the broader category of symbolic neural network architectures. There are multiple variants of polynomial neural networks. For a more detailed discussion on these architectures, interested readers can refer to the work of Grigorios G. Chrysos. In our study, we found Ref.³³'s π -net V1 to be the most effective, as illustrated in Fig 1. This architecture relies on Hadamard products⁷⁷ of linear layers without activation functions, denoted L_i :

$$L_i(x) = x * w_i + b_i \quad (5)$$

to construct higher-order polynomials. The architecture needs to be defined beforehand based on the desired degree of the

polynomial. There are no hyperparameters to tune within this architecture. A π -net can generate any n -degree polynomial for the given state variables. The hidden layers can be larger or smaller than the input layer, provided that the dimensions are compatible when performing the Hadamard product operation.

Polynomial neural Ordinary Differential Equations⁹ integrate polynomial neural networks into the neural ODE framework¹⁰. Because the output of a polynomial neural ODE is a direct mapping of the input via tensor and Hadamard products without involving nonlinear activation functions, symbolic mathematics can be applied to derive a symbolic expression of the network. In contrast, conventional neural networks and neural ODEs, which involve nonlinear activation functions, do not allow for direct recovery of symbolic equations.

When it comes to learning stiff ODEs and evaluating numerical methods, polynomial neural ODEs are advantageous neural networks for several key reasons. Unlike traditional neural networks, polynomial neural networks bypass the need for data normalization or standardization, making them easier to apply across diverse modeling paradigms. Additionally, the ability of polynomial neural ODEs to output quantities at various scales makes them particularly well-suited for stiff ODEs, where such flexibility is essential. Moreover, stiff ODEs often feature constants that vary across multiple orders of magnitude, a challenge that polynomial neural ODEs are uniquely equipped to manage.

B. Stiff ODEs

Stiff ODEs are a class of problems where explicit integration methods become highly inefficient due to stability constraints. Stiffness arises when there is a significant disparity in time scales within a system, often characterized by a large

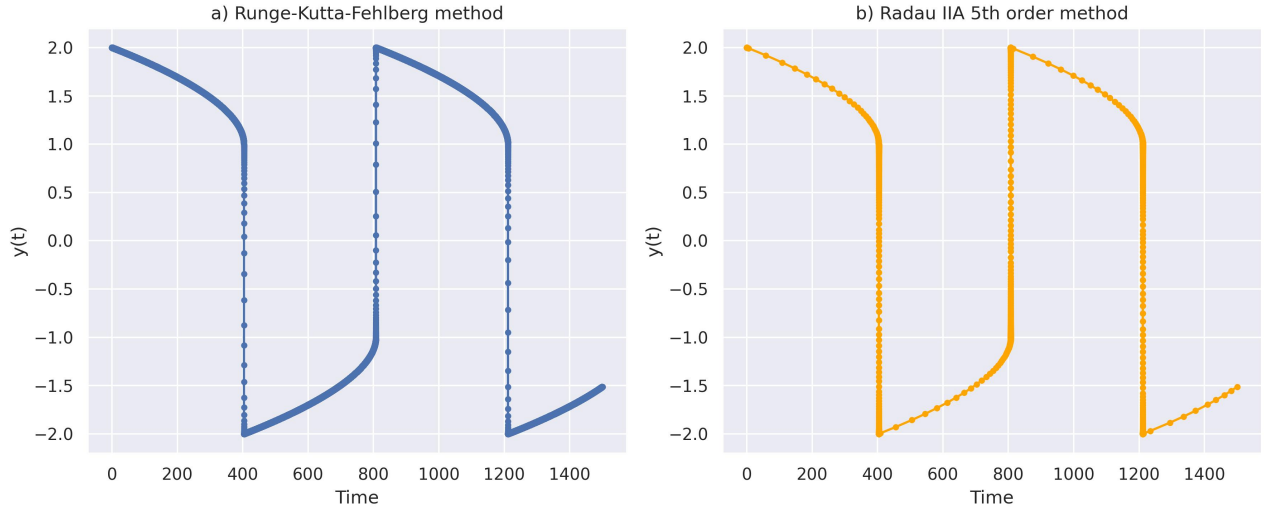


FIG. 2. Comparison of the integration of the deterministic stiff van der Pol oscillator with $\mu = 1000$ using two different methods: (a) explicit Runge-Kutta-Fehlberg, which is slow with 422,442 time points and 2,956,574 function evaluations, and (b) implicit Radau IIA 5th order, which is faster with only 857 time points and 7,123 function evaluations.

spread in the eigenvalues of the Jacobian matrix. To illustrate this, consider the stiff van der Pol oscillator with $\mu = 1000$ (Figure 2). Integrating this ODE using the explicit Runge-Kutta-Fehlberg method requires 422,442 data points to maintain stability, making the computation both slow and costly, taking several seconds to complete. In contrast, using an implicit scheme like the Radau IIA 5th order method reduces the number of data points to just 857, resulting in a much faster integration. While the number of data points provides some insight into computational cost, implicit methods involve iterative processes, so their true cost is not fully reflected in the number of time points. Therefore, the number of function evaluations is often a more accurate measure. In this example, the explicit Runge-Kutta-Fehlberg method required 2,956,574 function evaluations, while the Radau IIA 5th order method needed only 7,123, resulting in a significantly faster integration.

This example highlights the essence of stiffness in differential equations. For stiff problems, explicit methods demand extremely small time steps to ensure numerical stability, resulting in a substantial increase in computational cost. This is particularly problematic for neural ODEs, where thousands of integrations are needed during the training phase of a neural network. While explicit methods are easier to implement and have lower per-step costs, their inefficiency in handling stiffness makes them prohibitively slow for these applications. As a result, developing more efficient implicit solvers or novel approaches for neural ODEs is crucial to overcoming these limitations.

C. Discretize-Optimize vs. Optimize-Discretize

The Discretize-Optimize (Disc-Opt) and Optimize-Discretize (Opt-Disc) approaches are two fundamental

paradigms for optimizing neural ODEs. We visually illustrate the difference between the two approaches in Fig. 3 In the Disc-Opt approach, the ODE is first discretized, and then the optimization is performed directly on the discretized problem. This method is relatively straightforward to implement, particularly with the help of automatic differentiation tools that compute gradients efficiently⁶³. On the other hand, the Opt-Disc approach involves defining a continuous optimization problem and deriving the gradients in the continuous domain before discretizing the ODE. This requires solving the adjoint equation numerically, a process that is often more complex and computationally demanding⁶⁴.

Both Disc-Opt and Opt-Disc approaches face challenges, particularly in the computational costs associated with solving the ODE during forward propagation and calculating gradients via backpropagation in gradient-based optimization. Solving the forward propagation accurately demands significant memory and floating-point operations, potentially making training prohibitively expensive. While a lower-accuracy solver could theoretically speed up computations, this poses a problem for the Opt-Disc approach, where inaccurate forward propagation and adjoint solutions can degrade the quality of the gradients⁶⁵. In contrast, Disc-Opt does not suffer from this issue; the accuracy of the gradients is independent of the forward propagation’s accuracy, offering a compelling advantage for improving training efficiency. The Opt-Disc approach, which relies on adjoint methods that recompute the neural ODE backward in time, is also vulnerable to numerical instabilities, especially when dealing with stiff ODEs. These instabilities can significantly impact training performance and reliability.

Ref. 53 highlights several key findings that favor the Disc-Opt approach. First, it demonstrates that Disc-Opt achieves similar or even superior validation loss values at reduced computational costs compared to Opt-Disc. Specifically, the Disc-

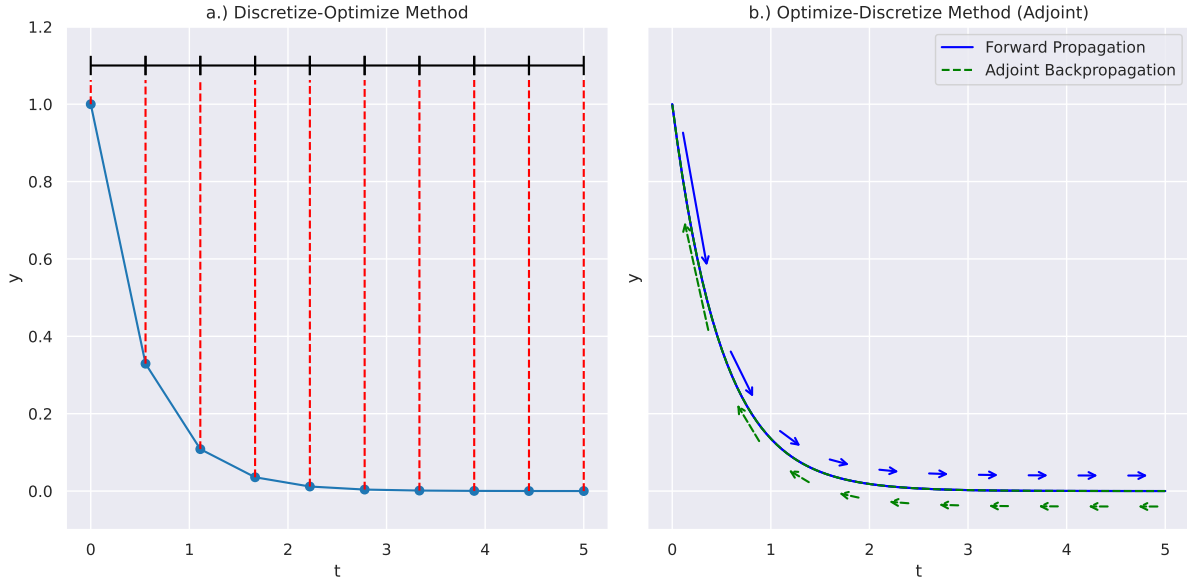


FIG. 3. Illustration of (a) Discretize-Optimize and (b) Optimize-Discretize methods. For Discretize-Optimize, black and red lines denote the discretized grid used to perform the optimization. For Optimize-Discretize, blue arrows indicate the forward pass of the neural network, while blue lines depict the backward pass using the adjoint method, illustrating how gradients are computed.

Opt method offers an average speedup of 20x over the Opt-Disc approach. This performance difference is partly due to the potential inaccuracies in gradients when using Opt-Disc methods, as also discussed by Ref. 65. In Opt-Disc, gradients can become unreliable if the state and adjoint equations are not solved with sufficient precision. Meanwhile, in Disc-Opt, the gradients remain accurate regardless of the solver’s accuracy, allowing the solver’s precision to be adjusted based on the data’s noise level, which is particularly useful in scientific applications. Given the substantial speed advantages of the Discretize-Optimize approach, we have prioritized this method over the adjoint method in our research. Our focus has been to understand the fundamentals of training stiff ODEs using various integration schemes and to leverage this knowledge to develop a new differential ODE solver that builds on these basics.

D. Numerical Methods for Solving ODEs

Single-step and multistep methods are two fundamental approaches for solving ordinary differential equations (ODEs). Single-step methods, like the Euler and Runge-Kutta schemes, compute the next solution value using only the information from the current step. This makes them relatively simple to implement and understand, as they do not depend on previous values of the solution. In contrast, multistep methods, such as Adams-Bashforth and Adams-Moulton methods, use information from several previous time steps to estimate the solution at the next point. While multistep methods can be more efficient in terms of computational cost per step for certain problems, they require careful management of past data

and have more complex stability properties. While multistep methods can be advantageous in some contexts, they introduce additional challenges compared to single-step methods.

Single-step methods are often the easiest to handle and grasp, making them an ideal starting point for developing integration methods for neural ODEs. Because they rely only on the current state, they provide a straightforward path for understanding the dynamics of neural ODEs and the process of backpropagation through the predicted ODE solution. Multistep methods, however, present challenges when applied to neural ODEs, particularly in the training phase. Since multistep methods depend on several past time points, initiating these methods requires multiple accurate previous points. Given that training data for neural networks may be noisy or incomplete, these required past points cannot always be directly used, and must instead be computed anew, adding complexity and slowing down the computation. Additionally, the need for multiple prior points complicates backpropagation, as gradients must be traced through the methods used to create previous values to initiate the method. These factors make single-step methods seem like the more practical and intuitive choice for initial research on neural ODEs, with multistep methods explored in future work once more foundational understanding is developed.

Single-Step Explicit Methods

Explicit methods are widely used for solving ordinary differential equations (ODEs) because of their straightforward implementation and lower computational cost per step. In these methods, the solution at the next time step is directly

calculated from the current step’s values, avoiding the need to solve nonlinear equations. This directness makes explicit methods computationally efficient for many problems, especially those that are non-stiff. Additionally, explicit methods are particularly cheap to use with neural ODEs because they can be backpropagated through very easily, allowing for efficient training of neural networks. However, when stiffness is involved, these methods often fall short.

The most basic explicit method is Euler’s method, which approximates the solution using a simple linear formula:

$$y_{n+1} = y_n + hf(t_n, y_n). \quad (6)$$

Here, y_{n+1} is the solution at the next time step, h is the step size, and $f(t_n, y_n)$ is the derivative of y at the current time step t_n . Euler’s method is easy to implement but comes with limitations: its first-order accuracy often necessitates extremely small step sizes to maintain accuracy, making it impractical for anything but the simplest, non-stiff problems.

The forward Euler method is most often used as a teaching tool or for problems where precision is not a critical factor. Although it is only first-order accurate, this method is commonly employed in many neural ODE applications during preliminary research when developing new methods, or when it is the only affordable option for specific use cases. For instance, MeshGraphNet⁶⁶, a graph neural network-based neural ODE capable of learning mesh-based multiphysics simulations like those in COMSOL, relies on the forward Euler method due to the high cost of backpropagating through its numerous graph neural network layers.

A more robust family of explicit methods are the Runge-Kutta (RK) methods, particularly the classical 4th-order Runge-Kutta method (RK4). Unlike Euler’s method, RK4 calculates the next value by considering a weighted average of several intermediate points within the current interval. The RK4 formula can be written as:

$$y_{n+1} = y_n + \frac{h}{6}(k_1 + 2k_2 + 2k_3 + k_4), \quad (7)$$

where

$$k_1 = f(t_n, y_n), \quad (8)$$

$$k_2 = f\left(t_n + \frac{h}{2}, y_n + \frac{h}{2}k_1\right), \quad (9)$$

$$k_3 = f\left(t_n + \frac{h}{2}, y_n + \frac{h}{2}k_2\right), \quad (10)$$

$$k_4 = f(t_n + h, y_n + hk_3). \quad (11)$$

This approach offers a good balance between computational cost and accuracy, making it popular in many applications requiring moderate precision. RK4, being a fourth-order method, is considerably more accurate than Euler’s method for a given step size and is better suited for a range of non-stiff problems.

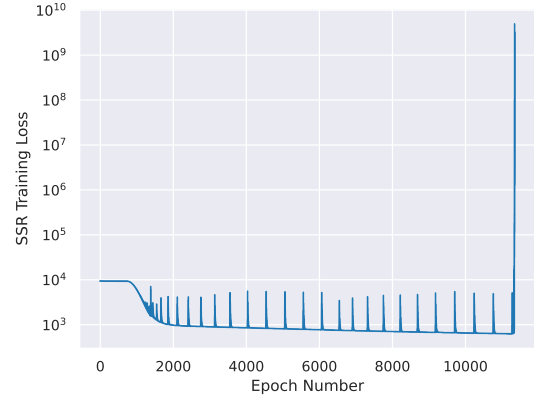


FIG. 4. Plot of the sum of squared residuals (SSR) training loss against epoch number for the stiff van der Pol model with $\mu = 1000$. The graph shows that the training becomes unstable as the neural ODE stiffens, causing the training to halt.

We demonstrate the limitations of explicit methods when training stiff neural ODEs using a specific example. We attempted to train a polynomial neural ODE on the dynamics of the stiff van der Pol oscillator with $\mu = 1000$, employing the classical 4th order Runge-Kutta method (Eq. 7) in a discretize-optimize framework with a fixed step size matching the interval between observed data points. Figure 4 presents the sum of squared residuals (SSR) training loss versus epoch number. The plot reveals that the training becomes unstable as the neural ODE develops stiffness, ultimately leading to a halt in the process.

While explicit methods like forward Euler method and RK4 are easier to implement and computationally cheaper per step, their inability to handle stiffness efficiently often makes them impractical for stiff ODEs. When faced with stiff problems, explicit methods require extremely small time steps to maintain stability, leading to prohibitively slow computation. This limitation drives the need for more complex but efficient alternatives like implicit methods.

Single-Step Implicit Methods

Implicit methods are a powerful solution to the challenges posed by stiff ODEs. Unlike explicit methods, which compute the next step directly from current values, implicit methods require solving a multivariate system of nonlinear equations at each step. This process is more computationally intensive, but it provides significantly greater stability, enabling the use of larger time steps without losing accuracy. The trade-off between computational cost and stability makes implicit methods particularly effective for stiff systems, but they tend to be slower for non-stiff ODEs where stability constraints are not a limiting factor.

The simplest implicit method is the backward Euler method:

$$y_{n+1} = y_n + hf(t_{n+1}, y_{n+1}), \quad (12)$$

which computes the solution, y_{n+1} , with a linear approximation of the derivative through the solution point. Since the value of y_{n+1} is unknown, a nonlinear system of equations must be solved with a root-finding method such as Newton's method, which substantially increases the computational cost. In some situations, the root-finding process may fail to converge, requiring an adjustment of the step size and resulting in further computational overhead.

The backward Euler method is A-stable, meaning that numerical errors do not grow uncontrollably. While it is only first-order accurate, the method's unconditional stability leads to stiff decay, where rapidly varying components decay quickly to zero, stabilizing the solution. An important feature of the backward Euler method is its ability to dampen oscillations effectively. When applied to stiff problems with oscillatory solutions, the backward Euler method tends to smooth out oscillations and drive the solution towards equilibrium. This strong damping effect is particularly beneficial in cases where spurious oscillations, which are common in neural ODEs due to the flexible nature of their approximating functions, can impact the accuracy or stability of the numerical solution, potentially leveraging stiff decay to mitigate these oscillations. However, this comes at the cost of potentially overdamping the solution, making it appear too smooth or slow to respond to changes, which can be problematic for models that inherently exhibit oscillatory behavior.

An alternative implicit method is the trapezoid method, which improves upon the backward Euler method by using the average of the derivatives at the current and next points to compute the solution:

$$y_{n+1} = y_n + \frac{h}{2} (f(t_n, y_n) + f(t_{n+1}, y_{n+1})). \quad (13)$$

The trapezoidal method is second-order accurate and A-stable. However, it is not L-stable, which means it does not guarantee that all transient modes will decay rapidly to zero. In practice, this can lead to less effective damping of very stiff components. Additionally, the trapezoid method can introduce oscillations into the solution. Since neural ODEs can become quite stiff during training, the trapezoidal method's potential to introduce oscillations may further intensify this stiffness. Because it uses an average of the derivative at two points, it does not dampen oscillations as aggressively as the backward Euler method. As a result, for problems where damping is crucial, the trapezoid method may allow small oscillations to persist, potentially leading to less stable behavior over long simulations.

The Radau IIA methods^{78–80}, belonging to the broader class of implicit Runge-Kutta methods, are among the most suitable high-order single-step implicit methods available. These methods are highly regarded for their exceptional stability, making them a preferred choice for solving highly stiff problems. Radau IIA methods are both A-stable and L-stable, which allows them to handle large step sizes while ensuring

that transient solutions decay quickly. Implicit Runge-Kutta methods have the following form:

$$Y_i = y_n + h \sum_{j=1}^s a_{ij} f(t_n + c_j h, Y_j), \quad i = 1, \dots, s, \quad (14)$$

$$y_{n+1} = y_n + h \sum_{j=1}^s b_j f(t_n + c_j h, Y_j) \quad (15)$$

where Y_i are the stage values, a_{ij} are the coefficients from the Butcher tableau, and c_j are the nodes. The Butcher tableau for Radau3 and Radau5 are shown in Fig.5 (see Ref. 80). This formulation requires solving a nonlinear system involving all stage values Y_i , which adds to the computational cost. However, the benefit of L-stability ensures that the stiff components of the solution decay without oscillation, making it ideal for highly stiff ODEs.

$\frac{1}{3}$	$\frac{5}{12}$	$-\frac{1}{12}$	$\frac{4-\sqrt{6}}{10}$	$\frac{88-7\sqrt{6}}{360}$	$\frac{296-169\sqrt{6}}{1800}$	$\frac{-2+3\sqrt{6}}{225}$
1	$\frac{3}{4}$	$\frac{1}{4}$	$\frac{4+\sqrt{6}}{10}$	$\frac{296+169\sqrt{6}}{1800}$	$\frac{88+7\sqrt{6}}{360}$	$\frac{-2-3\sqrt{6}}{225}$
	$\frac{3}{4}$	$\frac{1}{4}$	1	$\frac{16-\sqrt{6}}{36}$	$\frac{16+\sqrt{6}}{36}$	$\frac{1}{9}$
				$\frac{16-\sqrt{6}}{36}$	$\frac{16+\sqrt{6}}{36}$	$\frac{1}{9}$

FIG. 5. Butcher tableau for Radau IIA methods: (left) Radau3, (right) Radau5

E. Implicit Function Theorem

Backpropagation is the process of tracing a computational graph to compute gradients of a loss function with respect to model parameters, which is fundamental in training neural networks. In the context of training neural ODEs, explicit schemes such as the forward Euler or RK4 methods compute the solution at the next time step directly from the current values. This direct calculation creates a straightforward computational graph, making it easy to trace and backpropagate through each step. However, implicit schemes, like the backward Euler or Radau IIA methods, involve solving a nonlinear equation at each step to determine the next solution value. This nonlinear solver introduces a nested computational loop, which is both computationally expensive and can be numerically unstable when unrolling the entire loop during backpropagation. The result is a cumbersome and potentially error-prone process that significantly increases the computational burden.

The implicit function theorem provides an elegant solution to the challenge of backpropagating through an implicit scheme without needing to fully unroll the nonlinear iteration process. Once the root of the nonlinear equation is found using an implicit method, the implicit function theorem allows us to compute the gradient of the solution with respect to the inputs directly at this root.

We can reformulate our implicit scheme as an equation where we aim to find a root:

$$g(y_n, y_{n+1}, \theta) = 0. \quad (16)$$

For instance, the backward Euler method can be expressed in this form:

$$g(y_n, y_{n+1}, \theta) = y_{n+1} - y_n - hf(t_{n+1}, y_{n+1}, \theta) = 0. \quad (17)$$

To move our neural ODE solution forward by one time step, $t_{n+1} = t_n + h$, we solve Eqn 16 using Newton’s method for finding the root of a nonlinear equation:

$$y_{n+1}^{(v+1)} = y_{n+1}^{(v)} - \left(\frac{\partial g}{\partial y_{n+1}^{(v)}} \right)^{-1} g(y_n, y_{n+1}^{(v)}, \theta), \quad (18)$$

where v is the iteration number. After obtaining a prediction for the solution of our neural ODE, y_{n+1} , at the observed time point t_{n+1} , we need to compute the gradient of this prediction with respect to the model parameters, $\frac{\partial y_{n+1}}{\partial \theta}$, to update the neural network. While it is feasible to employ forward or reverse mode automatic differentiation to backpropagate directly through the multiple iterations of the root-finding process used to solve the implicit scheme, doing so is both computationally expensive and numerically unstable. Therefore, we take a different route: leveraging the implicit function theorem to compute the desired gradients:

$$\frac{\partial y_{n+1}}{\partial \theta} = - \left(\frac{\partial g}{\partial y_{n+1}} \right)^{-1} \frac{\partial g}{\partial \theta}. \quad (19)$$

The implicit function theorem expression is evaluated at the solution obtained from solving our nonlinear system of equations. If this solution is not sufficiently accurate, the resulting gradient calculation can become numerically unstable and imprecise. However, the additional gradients, $\frac{\partial g}{\partial y_{n+1}}$ and $\frac{\partial g}{\partial \theta}$, can be easily computed using automatic differentiation. Alternatively, analytical expressions for these gradients can be derived manually. It is also important to note that computing the inverse in Eqns 18 and 19 is known to be potentially numerically unstable. This instability can be mitigated by reformulating the inverse calculation as a linear system solution.

A simple outline of the algorithm for computing the solution and gradient for a single time step is presented in Algorithm 1. In summary, training neural ODEs with implicit schemes requires 1) solving the nonlinear system of equations defining the implicit scheme and 2) solving the linear system involved in the implicit function theorem. The computational expense of this method is primarily determined by the number of iterations required for Newton’s method to converge, the cost of calculating the necessary gradients, and the effort involved in solving the associated linear systems.

Algorithm 1 Implicit Scheme for a Single Time Step

Step 1: Solve the implicit equation $g(y_n, y_{n+1}, \theta) = 0$
a. Apply Newton’s iteration until convergence:

$$y_{n+1}^{(v+1)} = y_{n+1}^{(v)} - \left(\frac{\partial g}{\partial y_{n+1}^{(v)}} \right)^{-1} g(y_n, y_{n+1}^{(v)}, \theta)$$

Step 2: Calculate the gradient with the Implicit Function Theorem

$$\frac{\partial y_{n+1}}{\partial \theta} = - \left(\frac{\partial g}{\partial y_{n+1}} \right)^{-1} \frac{\partial g}{\partial \theta}$$

III. RESULTS

We begin by evaluating our methodology on the stiff univariate linear test equation (Example 1), a common benchmark in stability analysis across various ODE discretization schemes, making it a suitable first baseline. Next, we apply the methodology to two custom-designed stiff nonlinear models: a 2-dimensional system (Example 2) and a 3-dimensional system (Example 3). Due to the scarcity of well-established test models for stiff neural ODEs, we developed these toy models to explore the performance of our approach in addressing the challenges posed by stiffness in neural ODEs. Example 4, is the “High Irradiance RESponse” (HIRES) model, a widely used benchmark for evaluating ODE solver performance on stiff ordinary differential equations. For each model, we generated the corresponding training data. We then assessed the ability of the various single-step implicit schemes to recover the underlying ODE model under different training data conditions.

A. Example 1: Stiff Linear Model

In our first test, we consider the stiff linear equation:

$$\frac{dy}{dt} = -10000y, \quad y(0) = 1000, \quad t \in [0, 0.01]. \quad (20)$$

This equation, with solution plotted in Figure 6, serves as a standard example for evaluating the stability of numerical integration schemes in stiff systems. The high degree of stiffness, driven by the large negative coefficient, causes an initial rapid transient at the beginning of the time interval, followed by a smooth, slow decay as the system approaches equilibrium. This smooth behavior, which dominates most of the solution, represents the stiff region of the ODE. The one-dimensional nature of the model, along with its tunable stiffness parameter, provides a controlled setting to systematically evaluate integration schemes under varying stiffness conditions. By adjusting the stiffness, we can fine-tune the problem’s difficulty and assess the performance, stability, and accuracy of implicit solvers designed for stiff problems.

Given the stiffness of the problem, we generate the training data by integrating the initial value problem (IVP) using the Radau solver in SciPy⁸¹. Figure 6 shows the training data for the case with $n = 200$ data points equally spaced in time. As described in the methods section, following the

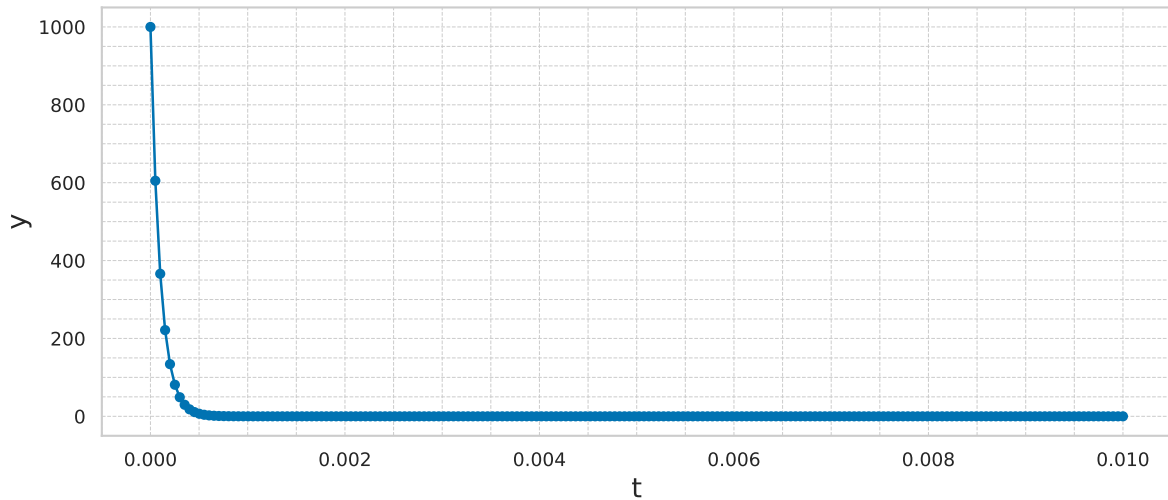


FIG. 6. For the equation $y' = -10000y$, we show the training data corresponding to an experiment consisting of 200 total data points equally spaced in time.

discretize-then-optimize approach, we partition the data into $n - 1$ training samples, each representing an IVP between two consecutive known data points. During each epoch, we solve these $n - 1$ IVPs simultaneously using our custom JAX^{82,83} implementation of the implicit schemes detailed in the methods section, enabling faster backpropagation through the ODE discretization process⁸⁴.

Using the training data, we trained a π -net V1 polynomial neural network to recover the underlying ODE equation. Table 1 shows the recovered equations for varying numbers of training data points equally spaced in time, for the four implicit schemes: backward Euler, trapezoid method, Radau3, and Radau5. To demonstrate the impact of the number of training data points on the ability to identify the underlying ODE, we plotted the parameter fractional relative error against the number of data points (see Figure 7). As expected, the recovered equations show a clear improvement with the use of higher-order methods, emphasizing the importance of higher-order methods for accurately integrating ODEs within the neural ODE framework.

$y' = -10000y$	
n	Equation Learned
Backward Euler	
50 $y' =$	$-32814.7600708y + 8.44726018571 \cdot 10^{-11}$
100 $y' =$	$-17284.1957884y - 6.65078880626 \cdot 10^{-12}$
200 $y' =$	$-12992.0930002y + 9.10992647337 \cdot 10^{-12}$
1000 $y' =$	$-10517.6269781y + 1.65232316322 \cdot 10^{-11}$
10000 $y' =$	$-10050.1721181y + 2.23615888785 \cdot 10^{-11}$
Trapezoid Method	
50 $y' =$	$-7546.32076209y - 4.25736335374 \cdot 10^{-12}$
100 $y' =$	$-9228.38069787y - 2.92238168648 \cdot 10^{-11}$
200 $y' =$	$-9794.7490243y + 1.16207823362 \cdot 10^{-8}$
1000 $y' =$	$-9991.65833324y + 4.60703162317 \cdot 10^{-12}$
10000 $y' =$	$-9999.91665083y - 4.69854345928 \cdot 10^{-11}$
Radau3	
50 $y' =$	$-9251.48316114y - 1.0589518914 \cdot 10^{-11}$
100 $y' =$	$-9885.79527641y - 6.93292052555 \cdot 10^{-12}$
200 $y' =$	$-9984.36246911y - 5.90851257248 \cdot 10^{-11}$
1000 $y' =$	$-9999.86426589y + 8.25230499684 \cdot 10^{-12}$
10000 $y' =$	$-9999.99986144y + 4.41857407072 \cdot 10^{-12}$
Radau5	
50 $y' =$	$-10042.9715925y - 5.81410253423 \cdot 10^{-11}$
100 $y' =$	$-10001.2886455y + 8.15234805477 \cdot 10^{-12}$
200 $y' =$	$-10000.0413085y - 2.43678163057 \cdot 10^{-11}$
1000 $y' =$	$-10000.0000137y - 1.01896661931 \cdot 10^{-11}$
10000 $y' =$	$-10000.0000000014y + 1.06509360321 \cdot 10^{-11}$

TABLE I. Comparison of recovered equations for $y' = -10000y$ with selected implicit single-step methods and varying number of training points (n) equally spaced in time over the time interval.

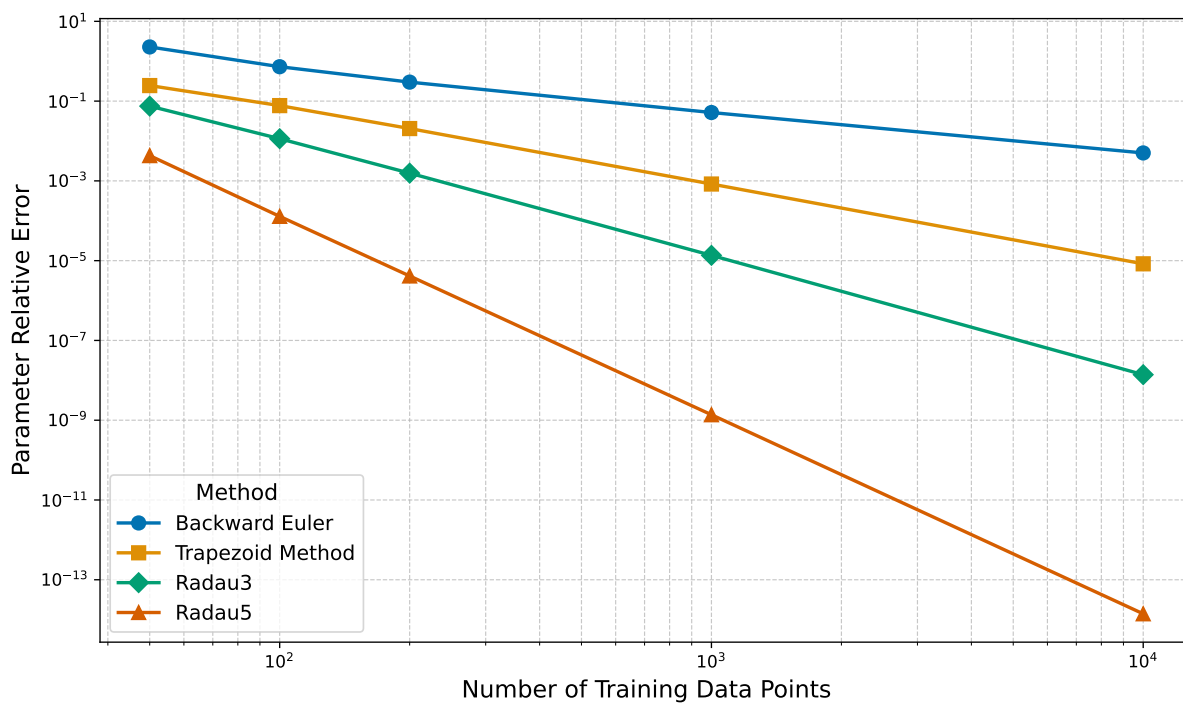


FIG. 7. For the equation $y' = -10000y$, we visualize the reduction in parameter relative error with more training data points for the Backward Euler, Trapezoid, Radau3, and Radau5 schemes.

B. Example 2: 2D Nonlinear Model

In our second example, we introduce the stiff nonlinear system:

$$\begin{aligned} \frac{dy_1}{dt} &= -10000y_1 + 100y_2^2, \\ \frac{dy_2}{dt} &= y_1 - y_2 - y_2^2, \\ y_1(0) &= 20, \quad y_2(0) = 20, \quad t \in [0, 1]. \end{aligned} \tag{21}$$

This system, plotted in Figure 8, was specifically designed to exhibit stiffness while containing only linear and quadratic terms. The presence of both linear decay and nonlinear coupling between the variables makes this model an ideal toy problem for testing stiff ODE system identification methods. By controlling the stiffness through the large coefficient on y_1 , we created a challenging yet tractable example that allows for detailed evaluation of numerical schemes in handling stiff nonlinear dynamics. This formulation provides a simple but effective framework for testing implicit solvers and their ability to recover underlying ODE models.

The training data for Example 2 was generated, and the neural ODE was trained using the same approach as described in Example 1, following the discretize-then-optimize framework. Table 2 provides a detailed comparison of the recovered equations across a range of data points and for the different single-step implicit schemes employed. This allows us to assess the accuracy and stability of each method as the number of training data points increases.

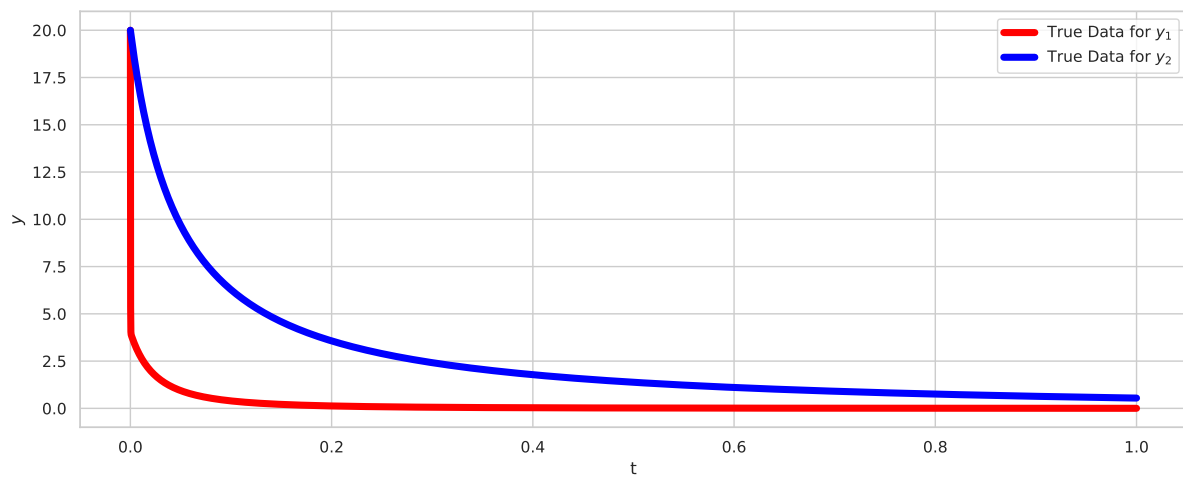


FIG. 8. The training data for Example 2 (see Eqn.21)

n	Equation Learned
$y_1' = -10000y_1 + 100y_2^2,$ $y_2' = y_1 - y_2 - y_2^2$	
Backward Euler	
577	$y_1' = 0.857790419745y_1^2 - 0.0272680143893y_1y_2 - 10166.4989566y_1 + 101.624836462y_2^2 + 0.386789183249y_2 - 0.551135993713$
	$y_2' = -0.285567838549y_1^2 + 0.0990745835285y_1y_2 + 4.71564636098y_1 - 1.05423705786y_2^2 - 0.986267801836y_2 - 0.0164417742954$
4376	$y_1' = 0.0423634999674y_1^2 - 0.0136574581553y_1y_2 - 10019.1933425y_1 + 100.193559849y_2^2 - 0.00554181653545y_2 + 0.00461000901951$
	$y_2' = 0.0139925781613y_1^2 - 0.00384030901297y_1y_2 + 0.866538777819y_1 - 0.999278346013y_2^2 - 1.00238051147y_2 + 0.000439112387467$
8751	$y_1' = 0.0364817641173y_1^2 - 0.0120205292793y_1y_2 - 10009.9663345y_1 + 100.096271379y_2^2 - 0.000862673544333y_2 - 0.00709106224596$
	$y_2' = -0.439927568256y_1^2 + 0.128016568173y_1y_2 + 6.75918777972y_1 - 1.06879499943y_2^2 - 0.974381990331y_2 - 0.0149734626991$
Trapezoid Method	
145	$y_1' = -0.423038447107y_1^2 - 0.403248762405y_1y_2 - 9979.491552y_1 + 99.8047902564y_2^2 - 0.689186448493y_2 + 0.800805937997$
	$y_2' = 0.22761623803y_1^2 - 0.0687649306312y_1y_2 - 2.41139781576y_1 - 0.958981780372y_2^2 - 1.0144592229y_2 + 0.009552131566691$
577	$y_1' = 0.0298776632968y_1^2 + 0.0181437044044y_1y_2 - 10000.1979833y_1 + 99.9956102994y_2^2 + 0.0452224334545y_2 - 0.05692000490361$
	$y_2' = -0.17024891461y_1^2 + 0.0512993520779y_1y_2 + 3.16217370708y_1 - 1.02616137055y_2^2 - 0.987906993242y_2 - 0.00733733298199$
4376	$y_1' = -0.000451671564475y_1^2 + 0.00014949629724y_1y_2 - 9999.98232229y_1 + 99.9998077655y_2^2 + 5.14818659507 \cdot 10^{-5}y_2 - 3.99846988559 \cdot 10^{-5}$
	$y_2' = 7.64828987695 \cdot 10^{-5}y_1^2 - 2.33820098112 \cdot 10^{-5}y_1y_2 + 0.998985271827y_1 - 0.999987315955y_2^2 - 1.00000444478y_2 + 3.36336098291 \cdot 10^{-6}$
Radau3	
20	$y_1' = -1.56632740236y_1^2 - 0.224103407018y_1y_2 - 9874.10782758y_1 + 99.0988980189y_2^2 - 3.5781048264y_2 + 4.91194004519$
	$y_2' = -0.0591948262252y_1^2 + 0.012507921399y_1y_2 + 1.74061008707y_1 - 1.0070012339y_2^2 - 0.992918470379y_2 - 0.00132397079369$
37	$y_1' = -0.120717060984y_1^2 + 0.194140379368y_1y_2 - 9987.85822282y_1 + 99.8650995746y_2^2 + 0.0589890982338y_2 + 0.0258256573482$
	$y_2' = -0.0150133355336y_1^2 + 0.00387787458166y_1y_2 + 1.19871123764y_1 - 1.00194072615y_2^2 - 0.998676793048y_2 - 0.000199589071681$
145	$y_1' = -0.00333024059846y_1^2 + 0.00111248227387y_1y_2 - 9999.73569034y_1 + 99.9974467188y_2^2 - 0.0003906683163161y_2 + 0.000125585915679$
	$y_2' = 0.00018120986925y_1^2 - 6.04045150265 \cdot 10^{-5}y_1y_2 + 0.995823855144y_1 - 0.999950004327y_2^2 - 1.00000294879y_2 + 8.95211376724 \cdot 10^{-6}$
Radau5	
11	$y_1' = -5.66608132241y_1^2 - 1.24035219594y_1y_2 - 9902.73108536y_1 + 99.3267715451y_2^2 - 1.37103956121y_2 + 1.03673055215$
	$y_2' = 0.00148133489004y_1^2 - 0.000260035218172y_1y_2 + 0.982538645216y_1 - 0.999805577828y_2^2 - 1.00004942722y_2 - 4.29412266605 \cdot 10^{-5}$
20	$y_1' = -0.132305045867y_1^2 - 0.0987991738869y_1y_2 - 9996.09479118y_1 + 99.9776184626y_2^2 - 0.0625012351374y_2 + 0.0242436057101$
	$y_2' = -0.00195871154822y_1^2 + 0.000601418050997y_1y_2 + 1.02339367357y_1 - 1.00028818765y_2^2 - 0.999853203255y_2 - 9.48991243202 \cdot 10^{-5}$
37	$y_1' = -0.00552818223261y_1^2 - 0.00545691268246y_1y_2 - 9999.79647512y_1 + 99.9988787042y_2^2 - 0.00488110731907y_2 + 0.00154592719858$
	$y_2' = 5.18117896271 \cdot 10^{-5}y_1^2 - 2.33054187013 \cdot 10^{-6}y_1y_2 + 0.997098804824y_1 - 0.999973205466y_2^2 - 0.999991266492y_2 - 8.01211279977 \cdot 10^{-6}$
145	$y_1' = -0.101757006641y_1^2 - 0.182511459523y_1y_2 - 9997.62782776y_1 + 99.9787763937y_2^2 - 0.266497871281y_2 + 0.300599770551$
	$y_2' = 0.116321371068y_1^2 - 0.0350215868825y_1y_2 - 0.653987981842y_1 - 0.980463029031y_2^2 - 1.00782026853y_2 + 0.00479238277096$
577	$y_1' = 0.0211250318694y_1^2 + 0.000558203885529y_1y_2 - 10000.5164523y_1 + 100.002550475y_2^2 + 0.0197394109923y_2 - 0.0253540979989$
	$y_2' = -0.110712807821y_1^2 + 0.0333953494942y_1y_2 + 0.994069819651y_1 - 1.01704469092y_2^2 - 0.992166957384y_2 - 0.0047840483542$

TABLE II. Comparison of recovered equations for Example 2 with selected implicit single-step methods and varying number of training points (n)

C. Example 3: 3D Nonlinear Model

In our third example, we consider the following stiff nonlinear system of ODEs:

$$\begin{aligned}
 \frac{dy_1}{dt} &= -500y_1 + 3.8y_2^2 + 1.35y_3, \\
 \frac{dy_2}{dt} &= 0.82y_1 - 24y_2 + 7.5y_3^2, \\
 \frac{dy_3}{dt} &= -0.5y_1^2 + 1.85y_2 - 6.5y_3^2, \\
 y_1(0) &= 15, \quad y_2(0) = 7, \quad y_3(0) = 10, \quad t \in [0, 5].
 \end{aligned} \tag{22}$$

This system, plotted in Figure 9, was constructed to be a more challenging stiff problem due to its three-dimensional nature while still consisting of only linear and quadratic terms. The increased dimensionality introduces more complex interactions between the variables, making this a more difficult test case for stiff ODE system identification methods. By incorporating both linear decay and nonlinear terms, this model provides a robust framework for evaluating the performance of integration schemes in handling stiff, higher-dimensional nonlinear dynamics.

The training data for Example 3 was generated, and the neural ODE was trained following the same procedure described for Example 1, utilizing the discretize-then-optimize framework. Tables 3, 4, 5, and 6 provide a detailed comparison of the recovered equations for varying numbers of data points (1467, 369, 94, and 48, respectively) and across the four chosen single-step implicit schemes.

Figure 10 plots the fractional relative error of the parameter against the number of data points, n . Similar trends are observed here as in Figure 7, indicating that the discretization scheme's order scales comparably for both the linear test problem and the higher-dimensional nonlinear ODE. This further highlights the significant improvement gained by employing higher-order methods, reinforcing the importance of such methods for accurately integrating ODEs in the neural ODE framework.

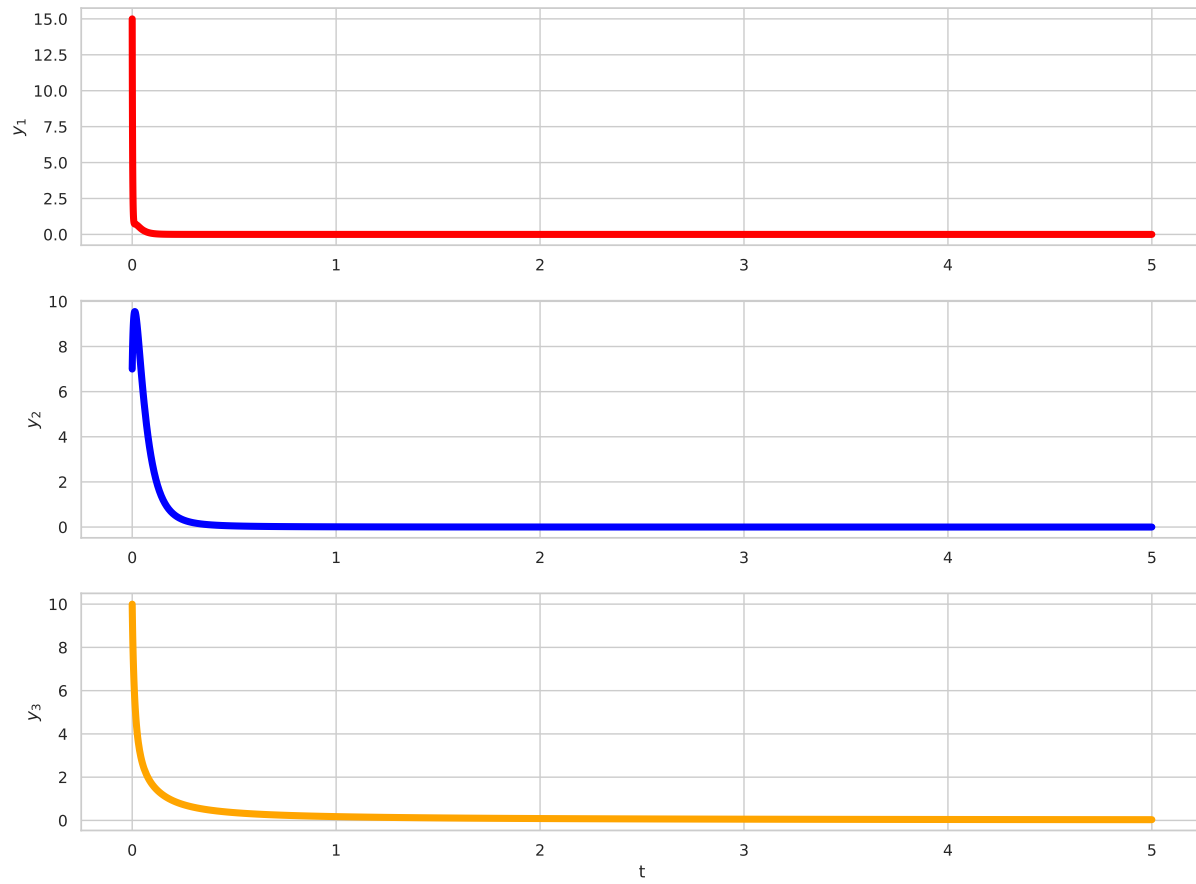


FIG. 9. The training data for Example 3 (see Eqn.22)

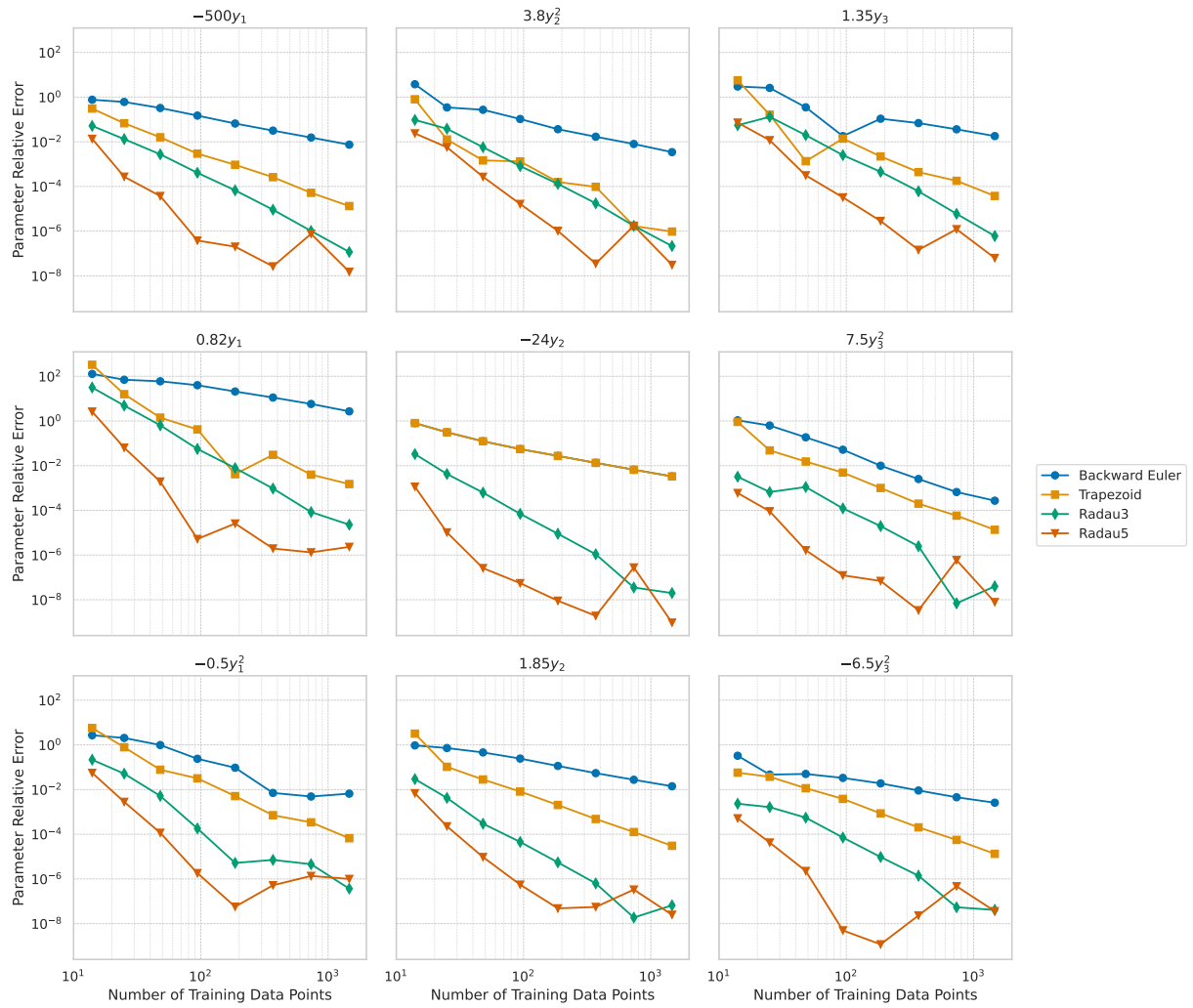


FIG. 10. For Example 3, we visualize the reduction in fractional parameter relative error (not a percentage) as a function of the number of training data points for the Backward Euler, Trapezoid, Radau3, and Radau5 integration schemes. The symbols displayed in the legend represent each integration method. The parameter reported in each subfigure corresponds to the specific term in the ODE, as indicated by the title of each subfigure.

n	Equation Learned
$y'_1 = -500y_1 + 3.8y_2^2 + 1.35y_3,$ $y'_2 = 0.82y_1 - 24y_2 + 7.5y_3^2,$ $y'_3 = -0.5y_1^2 + 1.85y_2 - 6.5y_3^2$	
Backward Euler	
1467 $y'_1 =$	$0.0384064527302y_1^2 + 0.204017196661y_1y_2 - 0.184501300028y_1y_3 - 503.719351023y_1 + 3.81306747361y_2^2$ $+ 0.030695277063y_2y_3 + 0.0138909801005y_2 - 0.0389371667798y_3^2 + 1.37431473228y_3 - 0.000981504457688$
$y'_2 =$	$0.0200787332271y_1^2 + 0.284950328409y_1y_2 + 0.00680359696552y_1y_3 - 1.3914960677y_1 + 0.0120642998079y_2^2$ $- 0.0039339966994y_2y_3 - 24.0794531237y_2 + 7.49797005252y_3^2 + 0.0118933425261y_3 - 0.000244780267862$
$y'_3 =$	$-0.503277229186y_1^2 - 0.0936986490342y_1y_2 - 0.0504958796953y_1y_3 + 0.969202527143y_1 - 0.000853834054426y_2^2$ $- 0.00916411500017y_2y_3 + 1.82402554075y_2 - 6.48322554439y_3^2 - 0.0124328526534y_3 + 0.000363525556554$
Trapezoid Method	
1467 $y'_1 =$	$-0.000214354771517y_1^2 - 0.000974387910813y_1y_2 + 0.00118871099339y_1y_3 - 499.993355185y_1 + 3.799999636531y_2^2$ $- 7.6389755885 \cdot 10^{-5}y_2y_3 - 6.49292906827 \cdot 10^{-5}y_2 + 0.00010856272938y_3^2 + 1.34994917202y_3 + 1.7778522614 \cdot 10^{-6}$
$y'_2 =$	$-9.40804457738 \cdot 10^{-5}y_1^2 - 0.000738401443738y_1y_2 + 0.000464830560082y_1y_3 + 0.821234592939y_1 - 4.98824711904 \cdot 10^{-6}y_2^2$ $- 4.45829770482 \cdot 10^{-5}y_2y_3 - 23.9998826649y_2 + 7.50010148624y_3^2 - 3.27328943583 \cdot 10^{-5}y_3 + 8.82781486984 \cdot 10^{-7}$
$y'_3 =$	$-0.499966869555y_1^2 + 0.000213011256539y_1y_2 + 2.40008585951 \cdot 10^{-5}y_1y_3 - 0.00124987034708y_1 - 2.79306256779 \cdot 10^{-6}y_2^2$ $+ 4.49476766209 \cdot 10^{-5}y_2y_3 + 1.85005644455y_2 - 6.50008628126y_3^2 + 4.10531838766 \cdot 10^{-5}y_3 - 1.29639482701 \cdot 10^{-6}$
Radau3	
1467 $y'_1 =$	$-1.58565658931 \cdot 10^{-6}y_1^2 - 9.0220800355 \cdot 10^{-6}y_1y_2 + 5.34341576966 \cdot 10^{-6}y_1y_3 - 499.999941385y_1 + 3.799999918096y_2^2$ $+ 2.82082509581 \cdot 10^{-6}y_2y_3 - 6.09956239295 \cdot 10^{-7}y_2 - 2.19977308688 \cdot 10^{-6}y_3^2 + 1.35000081713y_3 - 6.6422572823 \cdot 10^{-8}$
$y'_2 =$	$-4.10343797756 \cdot 10^{-7}y_1^2 - 7.61410752424 \cdot 10^{-7}y_1y_2 + 2.85277919953 \cdot 10^{-6}y_1y_3 + 0.819981280026y_1 + 1.08825064073 \cdot 10^{-7}y_2^2$ $- 3.29411976356 \cdot 10^{-7}y_2y_3 - 23.9999995232y_2 + 7.50000029772y_3^2 + 1.89809742021 \cdot 10^{-8}y_3 + 2.28812493605 \cdot 10^{-9}$
$y'_3 =$	$-0.499999816321y_1^2 + 1.05053334608 \cdot 10^{-6}y_1y_2 - 1.03391317172 \cdot 10^{-6}y_1y_3 + 1.56427731904 \cdot 10^{-6}y_1 - 9.58120432784 \cdot 10^{-8}y_2^2$ $+ 2.22479763452 \cdot 10^{-7}y_2y_3 + 1.85000012191y_2 - 6.50000026651y_3^2 + 6.09264676245 \cdot 10^{-8}y_3 - 2.12359008156 \cdot 10^{-9}$
Radau5	
1467 $y'_1 =$	$1.89090287095 \cdot 10^{-7}y_1^2 + 3.5678668997 \cdot 10^{-7}y_1y_2 - 1.2219774498 \cdot 10^{-6}y_1y_3 - 499.999992409y_1 + 3.79999988246y_2^2$ $+ 2.73754920441 \cdot 10^{-7}y_2y_3 - 1.14276913266 \cdot 10^{-7}y_2 - 1.86366762744 \cdot 10^{-7}y_3^2 + 1.35000008467y_3 - 5.43008217991 \cdot 10^{-9}$
$y'_2 =$	$9.91908825251 \cdot 10^{-8}y_1^2 + 3.35162036135 \cdot 10^{-7}y_1y_2 - 5.47629530017 \cdot 10^{-7}y_1y_3 + 0.820001899201y_1 - 5.11866915919 \cdot 10^{-8}y_2^2$ $+ 9.59397916389 \cdot 10^{-8}y_2y_3 - 23.9999999774y_2 + 7.49999994153y_3^2 + 1.62719936327 \cdot 10^{-8}y_3 + 1.13086047757 \cdot 10^{-8}$
$y'_3 =$	$-0.499999500734y_1^2 + 1.70838063042 \cdot 10^{-6}y_1y_2 - 2.67726935902 \cdot 10^{-6}y_1y_3 + 8.07912691944 \cdot 10^{-6}y_1 - 2.1660877351 \cdot 10^{-7}y_2^2$ $+ 3.46097651535 \cdot 10^{-7}y_2y_3 + 1.85000004597y_2 - 6.50000023501y_3^2 + 2.5045404555 \cdot 10^{-8}y_3 - 3.60211166233 \cdot 10^{-9}$

TABLE III. Comparison of recovered equations for Example 3 with selected implicit single-step methods and varying number of training points $n = 1467$

n	Equation Learned
$y'_1 = -500y_1 + 3.8y_2^2 + 1.35y_3,$ $y'_2 = 0.82y_1 - 24y_2 + 7.5y_3^2,$ $y'_3 = -0.5y_1^2 + 1.85y_2 - 6.5y_3^2$	
Backward Euler	
369	$y'_1 = 0.127904202437y_1^2 + 0.797524296352y_1y_2 - 0.618853828345y_1y_3 - 515.835938291y_1 + 3.86400911308y_2^2 + 0.100596632061y_2y_3 + 0.0702514281895y_2 - 0.144792011507y_3^2 + 1.44253523851y_3 - 0.00338565729602$ $y'_2 = 0.0543209089864y_1^2 + 1.04579692729y_1y_2 + 0.160430638587y_1y_3 - 8.37766824113y_1 + 0.0654796412269y_2^2 - 0.052630703619y_2y_3 - 24.3209270038y_2 + 7.51898512114y_3^2 + 0.0406798119831y_3 - 0.000613776339809$ $y'_3 = -0.503529354636y_1^2 - 0.329057521838y_1y_2 - 0.245153506381y_1y_3 + 3.85641129319y_1 - 0.00849774225915y_2^2 - 0.026326319065y_2y_3 + 1.74932608891y_2 - 6.44088493316y_3^2 - 0.048392901916y_3 + 0.00140276670564$
Trapezoid Method	
369	$y'_1 = -0.00268209780416y_1^2 - 0.0144329545699y_1y_2 + 0.0150266836908y_1y_3 - 499.869671739y_1 + 3.79963430099y_2^2 - 0.000501143645822y_2y_3 - 0.00134685668212y_2 + 0.00131751622372y_3^2 + 1.3494057239y_3 + 1.90847684559 \cdot 10^{-5}$ $y'_2 = -0.00114528900208y_1^2 - 0.0106000717948y_1y_2 + 0.00558187371416y_1y_3 + 0.84505905353y_1 - 0.000230229973003y_2^2 - 0.000472976562712y_2y_3 - 23.9980217168y_2 + 7.50149654194y_3^2 - 0.000524988587427y_3 + 4.37738386438 \cdot 10^{-5}$ $y'_3 = -0.499644737787y_1^2 + 0.00285307226783y_1y_2 + 0.00129595454858y_1y_3 - 0.0229524685876y_1 + 2.98567414682 \cdot 10^{-5}y_2^2 + 0.000590463049014y_2y_3 + 1.85089037745y_2 - 6.50132012361y_3^2 + 0.00064671327907y_3 - 2.36121005357 \cdot 10^{-5}$
Radau3	
369	$y'_1 = -7.61974773614 \cdot 10^{-5}y_1^2 - 0.000498327709512y_1y_2 + 0.000176699490206y_1y_3 - 499.995450213y_1 + 3.79993286416y_2^2 + 0.000217509049623y_2y_3 - 7.01297138472 \cdot 10^{-5}y_2 - 0.00017272660185y_3^2 + 1.35008196827y_3 - 7.79201917524 \cdot 10^{-6}$ $y'_2 = -1.12137698434 \cdot 10^{-5}y_1^2 - 2.36452610708 \cdot 10^{-5}y_1y_2 + 0.000100980310608y_1y_3 + 0.819221372929y_1 + 2.4231234723 \cdot 10^{-6}y_2^2 - 1.52392601319 \cdot 10^{-5}y_2y_3 - 23.9999739349y_2 + 7.50001854938y_3^2 + 1.28276717158 \cdot 10^{-7}y_3 + 1.54151826501 \cdot 10^{-7}$ $y'_3 = -2.499996445415y_1^2 + 8.11323903976 \cdot 10^{-6}y_1y_2 - 2.60051361773 \cdot 10^{-5}y_1y_3 + 0.000206368555709y_1 - 1.47477468822 \cdot 10^{-6}y_2^2 + 6.83199869368 \cdot 10^{-6}y_2y_3 + 1.84999882977y_2 - 6.50000902966y_3^2 + 3.08390275437 \cdot 10^{-6}y_3 - 1.29968263207 \cdot 10^{-7}$
Radau5	
369	$y'_1 = 2.30220329023 \cdot 10^{-7}y_1^2 + 1.54933629481 \cdot 10^{-7}y_1y_2 - 1.735114567 \cdot 10^{-6}y_1y_3 - 499.999986711y_1 + 3.79999986615y_2^2 + 3.27664762559 \cdot 10^{-7}y_2y_3 - 3.72090241285 \cdot 10^{-7}y_2 - 2.24252583531 \cdot 10^{-7}y_3^2 + 1.35000019644y_3 - 2.286440954572 \cdot 10^{-8}$ $y'_2 = -2.33773009214 \cdot 10^{-8}y_1^2 + 9.92538431166 \cdot 10^{-8}y_1y_2 + 1.3444454372 \cdot 10^{-7}y_1y_3 + 0.819998393109y_1 - 1.26758645632 \cdot 10^{-9}y_2^2 + 8.52471281065 \cdot 10^{-9}y_2y_3 - 23.9999999544y_2 + 7.4999999747y_3^2 + 2.87430402396 \cdot 10^{-9}y_3 + 9.91674265437 \cdot 10^{-10}$ $y'_3 = -0.499999739718y_1^2 + 1.17646454023 \cdot 10^{-6}y_1y_2 - 1.34311446085 \cdot 10^{-6}y_1y_3 + 1.82986355267 \cdot 10^{-6}y_1 - 1.20155537994 \cdot 10^{-7}y_2^2 + 1.87949702407 \cdot 10^{-7}y_2y_3 + 1.85000010274y_2 - 6.50000015111y_3^2 + 1.50549610304 \cdot 10^{-8}y_3 - 7.84295853547 \cdot 10^{-10}$

TABLE IV. Comparison of recovered equations for Example 3 with selected implicit single-step methods and varying number of training points $n = 369$

n	Equation Learned
$y'_1 = -500y_1 + 3.8y_2^2 + 1.35y_3,$ $y'_2 = 0.82y_1 - 24y_2 + 7.5y_3^2,$ $y'_3 = -0.5y_1^2 + 1.85y_2 - 6.5y_3^2$	
Backward Euler	
94	$y'_1 = 0.628429562731y_1^2 + 3.83347856227y_1y_2 - 2.44967509189y_1y_3 - 574.356843937y_1 + 4.19704419353y_2^2$ $- 0.0507037997737y_2y_3 + 0.639626711303y_2 - 0.173536682816y_3^2 + 1.37419372243y_3 + 0.029408755562$ $0.309621055396y_1^2 + 4.03977576762y_1y_2 + 0.137940498732y_1y_3 - 31.8965120786y_1 + 0.34747681308y_2^2$ $- 0.523025515187y_2y_3 - 25.3243973178y_2 + 7.88766384537y_3^2 + 0.00379946914356y_3 + 0.00975557096823$ $- 0.619343143732y_1^2 - 1.68702386966y_1y_2 - 0.365857735248y_1y_3 + 13.2374339888y_1 - 0.0081667697632y_2^2$ $- 0.090220830018y_2y_3 + 1.39932809859y_2 - 6.28447896663y_3^2 - 0.168276206228y_3 + 0.0038905402588$
Trapezoid Method	
94	$y'_1 = -0.0588646265565y_1^2 - 0.27012838604y_1y_2 + 0.345013331708y_1y_3 - 498.52567995y_1 + 3.80504335312y_2^2$ $- 0.0336776819517y_2y_3 - 0.0127434045842y_2 + 0.0397814247098y_3^2 + 1.33125963682y_3 + 0.000982572835436$ $- 0.0450668815737y_1^2 - 0.23297656984y_1y_2 + 0.244365221953y_1y_3 + 0.476040309876y_1 + 0.00869338753968y_2^2$ $- 0.0299121574977y_2y_3 - 23.9612707912y_2 + 7.53681178165y_3^2 - 0.0129193788573y_3 + 0.000718185923707$ $- 0.48410748181y_1^2 + 0.0805474244863y_1y_2 - 0.0356373166309y_1y_3 - 0.188145335786y_1 - 0.00387491084267y_2^2$ $+ 0.0159521980287y_2y_3 + 1.86508272955y_2 - 6.52489715182y_3^2 + 0.0109209453638y_3 - 0.000391914744422$
Radau3	
94	$y'_1 = -0.00365909221556y_1^2 - 0.02233368391164y_1y_2 + 0.0104314867655y_1y_3 - 499.795116702y_1 + 3.79689360939y_2^2$ $+ 0.00967601990744y_2y_3 - 0.00291843193932y_2 - 0.00759128716958y_3^2 + 1.3534044362y_3 - 0.000302176679636$ $- 0.000535842537473y_1^2 - 0.000757268154964y_1y_2 + 0.00536390419245y_1y_3 + 0.774043217656y_1 + 3.64111573268 \cdot 10^{-5}y_2^2$ $- 0.000681620496574y_2y_3 - 23.9983199818y_2 + 7.50092201196y_3^2 + 9.65683744741 \cdot 10^{-6}y_3 + 6.23666981312 \cdot 10^{-6}$ $y'_3 = -0.500090837014y_1^2 - 0.000436889453858y_1y_2 - 3.30120008436 \cdot 10^{-5}y_1y_3 + 0.0078554942054y_1 + 2.05865827988 \cdot 10^{-5}y_2^2$ $+ 0.000252612907303y_2y_3 + 1.8499162119y_2 - 6.50046305391y_3^2 + 0.000191341009964y_3 - 7.60979876269 \cdot 10^{-6}$
Radau5	
94	$y'_1 = -1.89033428846 \cdot 10^{-5}y_1^2 - 0.000170654975335y_1y_2 + 0.00012705069856y_1y_3 - 500.000190355y_1 + 3.800062444323y_2^2$ $- 0.000167896660251y_2y_3 - 4.18754513978 \cdot 10^{-5}y_2 + 0.000147243497995y_3^2 + 1.34995619502y_3 + 2.05245458063 \cdot 10^{-6}$ $y'_2 = -8.28386331835 \cdot 10^{-7}y_1^2 - 3.68832137414 \cdot 10^{-6}y_1y_2 + 3.09466147704 \cdot 10^{-6}y_1y_3 + 0.820004290117y_1 + 4.1506214355 \cdot 10^{-7}y_2^2$ $- 1.05453146239 \cdot 10^{-6}y_2y_3 - 23.9999986769y_2 + 7.50000092846y_3^2 - 2.10552301159 \cdot 10^{-6}y_3 - 9.00549707716 \cdot 10^{-8}$ $y'_3 = -0.500000911173y_1^2 + 2.07529363956 \cdot 10^{-6}y_1y_2 + 5.40416672462 \cdot 10^{-6}y_1y_3 - 5.55110292954 \cdot 10^{-5}y_1 + 2.65989297765 \cdot 10^{-7}y_2^2$ $- 5.62433858967 \cdot 10^{-7}y_2y_3 + 1.85000102497y_2 - 6.50000003228y_3^2 + 1.4512003836 \cdot 10^{-7}y_3 + 1.53771845539 \cdot 10^{-8}$

TABLE V. Comparison of recovered equations for Example 3 with selected implicit single-step methods and varying number of training points $n = 94$

n	Equation Learned
$y'_1 = -500y_1 + 3.8y_2^2 + 1.35y_3,$ $y'_2 = 0.82y_1 - 24y_2 + 7.5y_3^2,$ $y'_3 = -0.5y_1^2 + 1.85y_2 - 6.5y_3^2$	
Backward Euler	
48 $y'_1 =$	$1.82910880564y_1^2 + 8.77522528086y_1y_2 - 6.26048259683y_1y_3 - 662.79250133y_1 + 4.82816206628y_2^2$ $- 0.815104217543y_2y_3 + 1.67112795975y_2 + 0.37076347215y_3^2 + 0.880167900117y_3 + 0.12015687347$
$y'_2 =$	$0.821363180957y_1^2 + 6.93094406635y_1y_2 - 0.948084348591y_1y_3 - 48.1915891864y_1 + 0.863938300142y_2^2$ $- 1.60765034538y_2y_3 - 26.9635740125y_2 + 8.89368929416y_3^2 - 0.289151173692y_3 + 0.0411175673398$
$y'_3 =$	$-0.991176710831y_1^2 - 3.56810157187y_1y_2 + 0.754691504145y_1y_3 + 16.2729284742y_1 + 0.030668469293y_2^2$ $- 0.142692804358y_2y_3 + 1.0023097408y_2 - 6.17589039304y_3^2 - 0.280743480112y_3 + 0.00520012969419$
Trapezoid Method	
48 $y'_1 =$	$-0.241197044867y_1^2 - 1.20003110545y_1y_2 + 1.27269890609y_1y_3 - 492.058348031y_1 + 3.79442941946y_2^2$ $- 0.0365651879257y_2y_3 - 0.134839497026y_2 + 0.0728196465699y_3^2 + 1.35182703869y_3 - 0.00547754968617$
$y'_2 =$	$-0.173412349544y_1^2 - 0.896381372281y_1y_2 + 0.93067994678y_1y_3 - 0.339973344039y_1 + 0.0227551702672y_2^2$ $- 0.0841998788607y_2y_3 - 23.8484059563y_2 + 7.61494110899y_3^2 - 0.0396939701894y_3 + 0.00205575932009$
$y'_3 =$	$-0.46146772343y_1^2 + 0.221411627156y_1y_2 - 0.0322504040161y_1y_3 - 0.884561939734y_1 - 0.00166472898244y_2^2$ $+ 0.03410495033204y_2y_3 + 1.90210507435y_2 - 6.57477886428y_3^2 + 0.0386700013798y_3 - 0.00136341520966$
Radau3	
48 $y'_1 =$	$-0.00365909221556y_1^2 - 0.02233368391164y_1y_2 + 0.0104314867655y_1y_3 - 499.795116702y_1 + 3.79689360939y_2^2$ $+ 0.00967601990744y_2y_3 - 0.00291843193932y_2 - 0.00759128716958y_3^2 + 1.3534044362y_3 - 0.000302176679636$
$y'_2 =$	$-0.000535842537473y_1^2 - 0.000757268154964y_1y_2 + 0.00536390419245y_1y_3 + 0.774043217656y_1 + 3.64111573268 \cdot 10^{-5}y_2^2$ $- 0.000681620496574y_2y_3 - 23.9983199818y_2 + 7.50092201196y_3^2 + 9.65683744741 \cdot 10^{-6}y_3 + 6.23666981312 \cdot 10^{-6}$
$y'_3 =$	$-0.500090837014y_1^2 - 0.000436889453858y_1y_2 - 3.30120008436 \cdot 10^{-5}y_1y_3 + 0.0078554942054y_1 + 2.05865827988 \cdot 10^{-5}y_2^2$ $+ 0.000252612907303y_2y_3 + 1.8499162119y_2 - 6.50046305391y_3^2 + 0.000191341009964y_3 - 7.60979876269 \cdot 10^{-6}$
Radau5	
48 $y'_1 =$	$-1.89033428846 \cdot 10^{-5}y_1^2 - 0.000170654975335y_1y_2 + 0.00012705069856y_1y_3 - 500.000190355y_1 + 3.800062444323y_2^2$ $- 0.000167896660251y_2y_3 - 4.18754513978 \cdot 10^{-5}y_2 + 0.000147243497995y_3^2 + 1.34995619502y_3 + 2.05245458063 \cdot 10^{-6}$
$y'_2 =$	$-8.28386331835 \cdot 10^{-7}y_1^2 - 3.68832137414 \cdot 10^{-6}y_1y_2 + 3.09466147704 \cdot 10^{-6}y_1y_3 + 0.820004290117y_1 + 4.1506214355 \cdot 10^{-7}y_2^2$ $- 1.05453146239 \cdot 10^{-6}y_2y_3 - 23.9999986769y_2 + 7.50000092846y_3^2 - 2.10552301159 \cdot 10^{-6}y_3 - 9.00549707716 \cdot 10^{-8}$
$y'_3 =$	$-0.500000911173y_1^2 + 2.07529363956 \cdot 10^{-6}y_1y_2 + 5.40416672462 \cdot 10^{-6}y_1y_3 - 5.55110292954 \cdot 10^{-5}y_1 + 2.65989297765 \cdot 10^{-7}y_2^2$ $- 5.62433858967 \cdot 10^{-7}y_2y_3 + 1.85000102497y_2 - 6.50000003228y_3^2 + 1.4512003836 \cdot 10^{-7}y_3 + 1.53771845539 \cdot 10^{-8}$

TABLE VI. Comparison of recovered equations for Example 3 with selected implicit single-step methods and varying number of training points $n = 48$

D. Example 4: HIRES Model

In our fourth example, we consider the ‘‘High Irradiance RESponse’’ (HIRES) model:

$$\begin{aligned}
 \frac{dy_1}{dt} &= -1.71y_1 + 0.43y_2 + 8.32y_3 + 0.0007, \\
 \frac{dy_2}{dt} &= 1.71y_1 - 8.75y_2, \\
 \frac{dy_3}{dt} &= -10.03y_3 + 0.43y_4 + 0.035y_5, \\
 \frac{dy_4}{dt} &= 8.32y_2 + 1.71y_3 - 1.12y_4, \\
 \frac{dy_5}{dt} &= -1.745y_5 + 0.43y_6 + 0.43y_7, \\
 \frac{dy_6}{dt} &= -280y_6y_8 + 0.69y_4 + 1.71y_5 - 0.43y_6 + 0.69y_7, \\
 \frac{dy_7}{dt} &= 280y_6y_8 - 1.81y_7, \\
 \frac{dy_8}{dt} &= -280y_6y_8 + 1.81y_7, \\
 t &\in [0, 321.8122].
 \end{aligned}
 \tag{23}$$

This model is plotted in Figure 11. In this system of stiff ordinary differential equations (ODEs), the eight variables represent concentrations of chemical species in ‘‘high irradiance responses’’ of photomorphogenesis on the basis of phytochrome⁸⁵. This model is commonly used in numerical analysis to test ODE solvers’ ability to handle stiff and high-dimensional systems.

We generated our training data to emulate experimental results that a scientist might collect in a laboratory setting. First, we analyzed the model’s equations to determine plausible initial values for the eight chemical species. Using a Latin hypercube sampling^{86–89} approach, we systematically explored the space of possible initial conditions, generating 20 unique sets of initial values. Each set of initial conditions represents the starting concentrations for a different simulated experiment. The set of initial conditions we used to generate the training data can be found in table 7. The recovered equations for the training data using the Radau5 solver are presented in Tables 8 and 9. Due to the length of the equations, they have been split across two pages. For brevity, equations from other implicit solvers are not included. The results show that Radau5 performs well in reconstructing the model’s equation from the provided data.

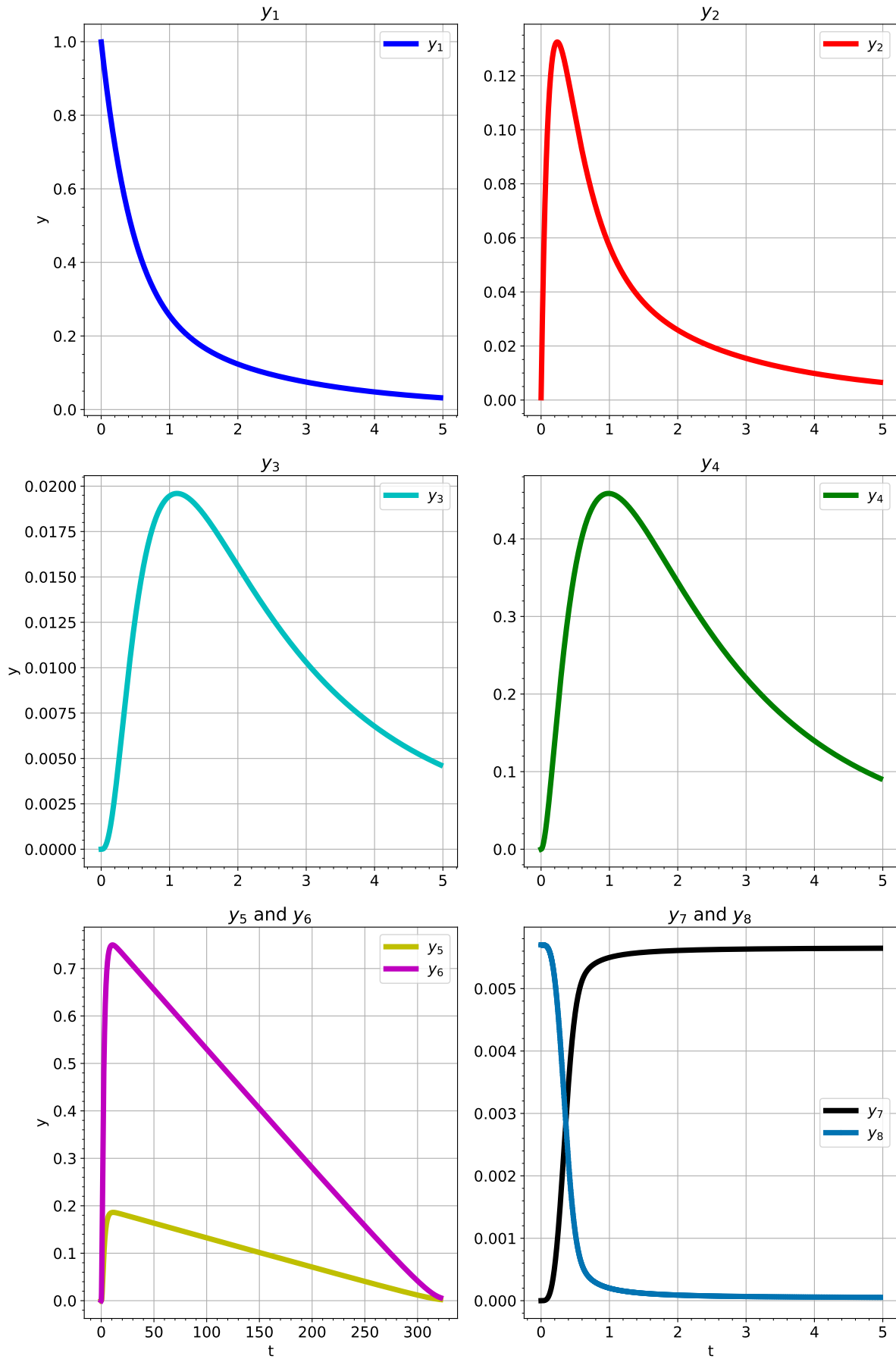


FIG. 11. The “High Irradiance Response” (HIRES) model

Initial Conditions for HIRES ODE Model								
Run	$y_1(0)$	$y_2(0)$	$y_3(0)$	$y_4(0)$	$y_5(0)$	$y_6(0)$	$y_7(0)$	$y_8(0)$
1	0.412503	0.906411	0.412933	0.213609	0.064925	0.293734	0.739312	0.043381
2	0.378101	0.391340	0.156641	0.503148	0.817612	0.433931	0.191203	0.007282
3	0.153447	0.071013	0.257224	0.455062	0.594616	0.367467	0.079906	0.047136
4	1.366815	0.236463	0.873612	0.893106	0.150143	0.115366	0.968644	0.000806
5	1.464978	0.993025	0.537866	0.611333	0.113295	0.245616	0.548675	0.009430
6	0.174331	0.570303	0.497073	0.406965	0.047271	0.616831	0.686488	0.012478
7	0.677526	0.659252	0.589131	0.925035	0.517411	0.966685	0.301191	0.029454
8	0.574262	0.329074	0.033387	0.339584	0.992378	0.006706	0.446191	0.022913
9	1.065735	0.518636	0.758506	0.998593	0.455977	0.483815	0.030678	0.004377
10	0.638101	0.703107	0.846135	0.816864	0.216076	0.860064	0.613366	0.019588
11	1.158734	0.012780	0.326158	0.561438	0.609144	0.518287	0.352820	0.034432
12	0.949418	0.460502	0.961568	0.157100	0.282788	0.075279	0.806771	0.040494
13	1.321282	0.269435	0.720024	0.122634	0.679448	0.838694	0.291664	0.025704
14	0.802005	0.760407	0.901060	0.000216	0.427964	0.304100	0.116146	0.031622
15	0.486976	0.815268	0.606734	0.081858	0.338174	0.582653	0.571258	0.014153
16	0.792132	0.410891	0.392693	0.374081	0.764888	0.188351	0.923021	0.035935
17	1.234614	0.605145	0.671905	0.660786	0.899778	0.751559	0.237024	0.015888
18	1.082288	0.150662	0.070913	0.270047	0.362950	0.731098	0.485404	0.049797
19	0.302551	0.136653	0.118964	0.763691	0.746139	0.900857	0.791212	0.022706
20	0.895915	0.886628	0.236694	0.705427	0.934826	0.652669	0.889384	0.038102

TABLE VII. This table presents the 20 initial conditions generated using Latin hypercube sampling, covering a wide range of plausible values for the eight chemical species in the HIRES model. These values emulate experimental results that a scientist might collect in a laboratory environment.

HIRES ODE Model
$ \begin{aligned} y_1' = & -0.00031073y_1^2 - 0.000464744y_1y_2 + 0.00056745y_1y_3 + 0.000425237y_1y_4 + 0.000642993y_1y_5 - 0.000404027y_1y_6 - 0.000331927y_1y_7 + 0.00354599y_1y_8 \\ & - 1.71007y_1 - 0.000205748y_2^2 + 0.000554287y_2y_3 - 0.00068709y_2y_4 + 0.000116956y_2y_5 + 0.000236726y_2y_6 + 0.000481911y_2y_7 - 0.0258092y_2y_8 \\ & + 0.431376y_2 - 0.000668385y_3^2 + 0.000693461y_3y_4 - 0.00192934y_3y_5 + 0.00193338y_3y_6 - 0.0018917y_3y_7 + 0.0411313y_3y_8 + 8.3202y_3 \\ & - 9.22908 \cdot 10^{-5}y_4^2 - 0.000850157y_4y_5 + 0.000271054y_4y_6 + 0.000537816y_4y_7 - 3.50722 \cdot 10^{-5}y_4y_8 - 0.000125337y_4 - 7.67578 \cdot 10^{-5}y_5^2 + 0.000287411y_5y_6 \\ & + 0.00028077y_5y_7 - 0.0110391y_5y_8 + 0.000852716y_5 - 3.76365 \cdot 10^{-5}y_6^2 - 0.000148388y_6y_7 + 0.0059082y_6y_8 - 0.000299744y_6 - 0.000258226y_7^2 \\ & + 0.0029199y_7y_8 - 8.96933 \cdot 10^{-5}y_7 + 4.74356 \cdot 10^{-5}y_8 - 5.63969 \cdot 10^{-5}y_8 + 0.000757073 \\ y_2' = & 9.69602 \cdot 10^{-5}y_1^2 + 0.000769587y_1y_2 - 0.000737449y_1y_3 - 7.12442 \cdot 10^{-7}y_1y_4 + 6.0849 \cdot 10^{-5}y_1y_5 - 0.000209591y_1y_6 - 0.000276887y_1y_7 - 0.00333511y_1y_8 \\ & + 1.71022y_1 + 9.28453 \cdot 10^{-5}y_2^2 - 0.00403004y_2y_3 - 0.000736836y_2y_4 - 0.000924404y_2y_5 + 0.000608029y_2y_6 + 0.000206462y_2y_7 - 0.0029632y_2y_8 \\ & - 8.7515y_2 + 0.00026641y_3^2 + 0.000996631y_3y_4 + 0.00085146y_3y_5 - 0.000289278y_3y_6 + 0.00010645y_3y_7 + 0.00954097y_3y_8 + 0.00374668y_3 \\ & + 6.40933 \cdot 10^{-5}y_4^2 + 0.000243817y_4y_5 + 6.69122 \cdot 10^{-6}y_4y_6 + 5.86059 \cdot 10^{-5}y_4y_7 + 0.00484422y_4y_8 - 0.00020343y_4 + 0.000230069y_5^2 - 0.000121354y_5y_6 \\ & - 5.42976 \cdot 10^{-5}y_5y_7 + 0.00126313y_5y_8 - 3.15179 \cdot 10^{-5}y_5 - 1.85762 \cdot 10^{-5}y_6^2 - 6.09471 \cdot 10^{-5}y_6y_7 - 0.0067078y_6y_8 + 0.000102471y_6 - 4.20929 \cdot 10^{-5}y_7^2 \\ & - 0.0012743y_7y_8 + 3.25278 \cdot 10^{-5}y_7 - 5.13354 \cdot 10^{-5}y_8^2 + 0.000105534y_8 + 4.51164 \cdot 10^{-5} \\ y_3' = & 0.000378181y_1^2 - 0.000201728y_1y_2 + 6.81887 \cdot 10^{-5}y_1y_3 - 0.000607169y_1y_4 - 0.000795986y_1y_5 - 6.13648 \cdot 10^{-5}y_1y_6 - 0.000681297y_1y_7 - 0.00019233y_1y_8 \\ & + 0.000506146y_1 + 0.000857537y_2^2 - 0.0027896y_2y_3 + 0.00175355y_2y_4 - 0.0011471y_2y_5 + 0.000923113y_2y_6 + 5.16552 \cdot 10^{-5}y_2y_7 + 0.00621137y_2y_8 \\ & - 4.08996 \cdot 10^{-5}y_2 + 0.00455072y_3^2 - 0.000775369y_3y_4 + 0.00357838y_3y_5 - 0.00272204y_3y_6 + 0.00333069y_3y_7 - 0.0295593y_3y_8 - 10.0342y_3 \\ & + 0.000137735y_4^2 + 0.000749415y_4y_5 + 3.16029 \cdot 10^{-5}y_4y_6 + 0.000135571y_4y_7 + 0.00431988y_4y_8 + 0.429673y_4 - 0.000408209y_5^2 - 0.000533999y_5y_6 \\ & - 0.000286398y_5y_7 + 0.00336681y_5y_8 + 0.0355456y_5 + 0.000117252y_6^2 + 0.000189377y_6y_7 - 0.00895939y_6y_8 - 7.3646 \cdot 10^{-6}y_6 + 0.000116177y_7^2 \\ & - 0.00208905y_7y_8 - 0.000133167y_7 - 7.93193 \cdot 10^{-5}y_8^2 + 8.18204 \cdot 10^{-5}y_8 - 7.64353 \cdot 10^{-5} \\ y_4' = & -0.000469981y_1^2 + 0.00123696y_1y_2 - 0.000795222y_1y_3 + 0.000329778y_1y_4 + 0.000426956y_1y_5 - 0.000401195y_1y_6 + 8.96783 \cdot 10^{-5}y_1y_7 - 0.00111913y_1y_8 \\ & + 0.000860503y_1 + 0.00122789y_2^2 + 0.0019002y_2y_3 - 0.00227422y_2y_4 + 0.000863651y_2y_5 - 0.000875247y_2y_6 - 0.00110464y_2y_7 - 0.00437968y_2y_8 \\ & + 3.31909y_2 + 0.000266218y_3^2 + 8.58294 \cdot 10^{-5}y_3y_4 - 0.00163539y_3y_5 + 0.00242771y_3y_6 - 0.00077684y_3y_7 + 0.0233927y_3y_8 + 1.70829y_3 \\ & + 9.00121 \cdot 10^{-5}y_4^2 - 0.000390212y_4y_5 + 0.000216153y_4y_6 + 0.000157371y_4y_7 - 0.00234737y_4y_8 - 1.12036y_4 + 0.00032589y_5^2 + 0.000273736y_5y_6 \\ & + 0.000467679y_5y_7 - 0.025374y_5y_8 - 0.000265808y_5 - 4.10952 \cdot 10^{-5}y_6^2 - 0.000194282y_6y_7 + 0.0122789y_6y_8 - 0.000103747y_6 - 6.4008 \cdot 10^{-5}y_7^2 \\ & + 0.00858852y_7y_8 + 3.28187 \cdot 10^{-5}y_7 + 7.18798 \cdot 10^{-5}y_8^2 - 9.19274 \cdot 10^{-5}y_8 - 2.31382 \cdot 10^{-5} \end{aligned} $

TABLE VIII. Comparison of learned equations for the HIRES ODE model with Radau5 solver. Variables y_1 through y_4 are displayed here, while y_5 through y_8 are provided separately in Table 9.

HIRES ODE Model
$ \begin{aligned} y_5' &= 0.00029978y_1^2 - 0.000591248y_1y_2 - 0.000378172y_1y_3 - 0.000100249y_1y_4 + 0.00130566y_1y_5 - 0.000650067y_1y_6 - 1.62772 \cdot 10^{-5}y_1y_7 + 0.000987743y_1y_8 \\ &- 0.000248203y_1 - 0.000176246y_2^2 - 0.00156651y_2y_3 + 0.000844348y_2y_4 - 0.00164954y_2y_5 + 0.00260392y_2y_6 + 0.000384903y_2y_7 - 0.000902123y_2y_8 \\ &- 0.0039323y_2 - 0.00173516y_3^2 - 0.00033139y_3y_4 + 0.00135832y_3y_5 - 0.00201798y_3y_6 + 5.06473 \cdot 10^{-5}y_3y_7 - 0.00637064y_3y_8 + 0.00709896y_3 \\ &+ 0.000142905y_4^2 - 0.000368813y_4y_5 + 7.86182 \cdot 10^{-5}y_4y_6 - 0.000191283y_4y_7 + 0.0013854y_4y_8 + 2.40603 \cdot 10^{-6}y_4 - 0.0007032y_5^2 - 4.41397 \cdot 10^{-5}y_5y_6 \\ &- 0.000656889y_5y_7 + 0.0106529y_5y_8 - 1.74446y_5 + 4.53541 \cdot 10^{-5}y_6^2 + 0.000306082y_6y_7 - 0.00422234y_6y_8 + 0.429853y_6 + 0.000482957y_7^2 \\ &- 0.00350062y_7y_8 + 0.429676y_7 + 1.59946 \cdot 10^{-5}y_8^2 + 6.95443 \cdot 10^{-6}y_8 + 3.7469 \cdot 10^{-6} \\ y_6' &= -0.000601099y_1^2 + 0.0029389y_1y_2 + 0.00385774y_1y_3 + 0.00108706y_1y_4 + 0.00184061y_1y_5 - 0.00174593y_1y_6 - 0.000432424y_1y_7 - 0.016071y_1y_8 \\ &- 0.000533911y_1 - 0.00405164y_2^2 + 0.000165568y_2y_3 - 0.00427113y_2y_4 - 0.00302155y_2y_5 + 0.00706652y_2y_6 + 0.00109165y_2y_7 + 0.031877y_2y_8 \\ &- 7.34781 \cdot 10^{-5}y_2 - 0.00065922y_3^2 + 0.00146815y_3y_4 - 0.0039533y_3y_5 + 0.000169268y_3y_6 - 0.00200273y_3y_7 + 0.0483894y_3y_8 - 0.000699031y_3 \\ &- 0.000388194y_4^2 - 0.00189157y_4y_5 + 0.000709487y_4y_6 + 0.00049555y_4y_7 - 0.00257293y_4y_8 + 0.690273y_4 - 0.000350412y_5^2 + 8.14434 \cdot 10^{-6}y_5y_6 \\ &+ 0.000238423y_5y_7 - 0.0234619y_5y_8 + 1.71098y_5 + 7.52056 \cdot 10^{-5}y_6^2 - 1.34922 \cdot 10^{-5}y_6y_7 - 279.821y_6y_8 - 0.43081y_6 + 2.55444 \cdot 10^{-5}y_7^2 \\ &+ 0.00681425y_7y_8 + 0.689092y_7 - 4.59914 \cdot 10^{-7}y_8^2 - 0.000278937y_8 + 0.00012531 \\ y_7' &= 0.00050809y_1^2 - 0.00303574y_1y_2 - 0.0018173y_1y_3 - 0.0016006y_1y_4 - 0.00297868y_1y_5 + 0.00126918y_1y_6 - 0.000171095y_1y_7 + 0.0153177y_1y_8 \\ &+ 0.00132467y_1 + 0.00319281y_2^2 + 0.0037057y_2y_3 + 0.00445928y_2y_4 + 0.00118958y_2y_5 - 0.00280684y_2y_6 + 0.000383333y_2y_7 + 0.00102508y_2y_8 \\ &+ 0.00806218y_2 + 0.000324329y_3^2 - 0.0010709y_3y_4 + 0.00534598y_3y_5 - 0.00267534y_3y_6 + 0.0013927y_3y_7 - 0.0783409y_3y_8 - 0.0144667y_3 \\ &+ 0.000212947y_4^2 + 0.00192085y_4y_5 - 0.000611197y_4y_6 - 0.000283165y_4y_7 - 0.000110696y_4y_8 - 0.000329872y_4 + 0.000941256y_5^2 - 0.000428766y_5y_6 \\ &- 0.000982112y_5y_7 + 0.0262727y_5y_8 - 0.000405728y_5 - 1.32294 \cdot 10^{-6}y_6^2 + 0.000262394y_6y_7 + 279.931y_6y_8 + 0.000711589y_6 + 0.000400862y_7^2 \\ &- 0.00724075y_7y_8 - 1.80995y_7 - 1.52332 \cdot 10^{-5}y_8^2 + 0.000205972y_8 - 0.000152767 \\ y_8' &= -0.000565499y_1^2 + 0.0030671y_1y_2 + 0.00160241y_1y_3 + 0.00153556y_1y_4 + 0.0030205y_1y_5 - 0.00131495y_1y_6 + 0.000169657y_1y_7 - 0.0148854y_1y_8 \\ &- 0.00119615y_1 - 0.00308975y_2^2 - 0.00391313y_2y_3 - 0.00420688y_2y_4 - 0.001022207y_2y_5 + 0.00278786y_2y_6 - 0.000499395y_2y_7 - 0.000913287y_2y_8 \\ &- 0.0094768y_2 - 0.000256329y_3^2 + 0.00101248y_3y_4 - 0.00551322y_3y_5 + 0.00267117y_3y_6 - 0.0014866y_3y_7 + 0.0784615y_3y_8 + 0.0162695y_3 \\ &- 0.000193634y_4^2 - 0.00186221y_4y_5 + 0.000639667y_4y_6 + 0.000315258y_4y_7 - 0.000629485y_4y_8 + 0.000204556y_4 - 0.000943349y_5^2 + 0.000527474y_5y_6 \\ &+ 0.00086977y_5y_7 - 0.0243707y_5y_8 + 0.000448275y_5 - 2.24672 \cdot 10^{-5}y_6^2 - 0.00031471y_6y_7 - 280.012y_6y_8 - 0.000723213y_6 - 0.000422873y_7^2 \\ &+ 0.0065505y_7y_8 + 1.81056y_7 + 1.42239 \cdot 10^{-5}y_8^2 - 0.000208139y_8 + 0.000154926 \end{aligned} $

TABLE IX. Comparison of learned equations for the HIRES ODE model with Radau5 solver. Variables y_4 through y_8 are displayed here, while y_1 through y_4 are provided separately in Table 8.

IV. CONCLUSION

This work introduces an approach to directly training stiff neural ordinary differential equations (ODEs). Earlier approaches for handling stiff neural ODEs relied on workarounds like equation scaling and regularization, which can help ODE solvers cope with stiffness temporarily but fail to offer a direct solution for training stiff neural ODEs. In contrast, our approach initiates the development of numerical methods specifically designed to manage stiffness without altering the original equations. This foundational step is key to creating robust and differentiable ODE solvers that can be applied across a wide range of fields, including partial differential equations (PDEs), physics-informed neural networks (PINNs), and mesh-based simulations such as MeshGraphNets.

In this paper, we focused on utilizing single-step implicit schemes to train stiff neural ODEs, which determine the next solution state based solely on the current one. These methods provide a simple yet effective approach to resolving the dynamics of stiff neural ODEs, while enabling efficient back-propagation through the ODE solutions via the implicit function theorem. Although we concentrated on single-step methods due to their simplicity and ease of implementation, more advanced multistep methods may offer computational advantages. However, multistep approaches depend on accurate information from several previous time points, complicating their use in neural ODE training. Future work will explore these multistep techniques and assess their potential benefits for managing stiffness.

Our experiments demonstrated successful training and accurate recovery of stiff ODE dynamics using several single-step implicit methods, including backward Euler, the trapezoid method, Radau3, and Radau5. While these methods effectively handled stiffness, they also introduced computational challenges. Implicit methods require solving a nonlinear system at each time step, which can be computationally expensive, especially for high-dimensional systems or when many iterations are necessary for convergence. As system dimensionality increases, these convergence issues become more pronounced, leading to an important open-ended research question: are there more efficient methods beyond the classical single-step implicit schemes commonly used in scientific computing?

In conclusion, this work shows that directly addressing stiffness in neural ODEs is not only feasible but also critical for expanding the use of neural ODEs. By confronting stiffness directly, we open up new possibilities for developing more robust, efficient, and versatile solvers, making neural ODEs suitable for tackling complex, real-world problems in a variety of scientific and engineering domains.

V. ACKNOWLEDGEMENTS

The authors acknowledge research funding from NIBIB Award No. 2-R01-EB014877-04A1 (grant 2-R01-EB014877-04A1 to LRP). Use was made of computational facilities

purchased with funds from the National Science Foundation (CNS-1725797) and administered by the Center for Scientific Computing (CSC). The CSC is supported by the California NanoSystems Institute and the Materials Research Science and Engineering Center (MRSEC; NSF DMR 1720256) at UC Santa Barbara. This work was supported in part by NSF awards CNS-1730158, ACI-1540112, ACI-1541349, OAC-1826967, OAC-2112167, CNS-2120019, the University of California Office of the President, and the University of California San Diego's California Institute for Telecommunications and Information Technology/Qualcomm Institute. Thanks to CENIC for the 100Gbps networks. The content of the information does not necessarily reflect the position or the policy of the funding agencies, and no official endorsement should be inferred. The funders had no role in study design, data collection and analysis, decision to publish, or preparation of the manuscript.

- ¹S. L. Brunton, J. L. Proctor, and J. N. Kutz, "Discovering governing equations from data by sparse identification of nonlinear dynamical systems," *Proceedings of the National Academy of Sciences* **113**, 3932–3937 (2016).
- ²S. Hirsh, D. Barajas-Solano, and J. Kutz, "Sparsifying priors for bayesian uncertainty quantification in model discovery," *Royal Society open science* **9**, 211823 (2022).
- ³K. Kaheman, J. N. Kutz, and S. L. Brunton, "Sindy-pi: a robust algorithm for parallel implicit sparse identification of nonlinear dynamics," *Proceedings. Mathematical, Physical, and Engineering Sciences* **476** (2020).
- ⁴S. Rudy, S. Brunton, J. Proctor, and J. Kutz, "Data-driven discovery of partial differential equations," *Science Advances* **3** (2016), 10.1126/sciadv.1602614.
- ⁵E. P. Alves and F. Fiuza, "Robust data-driven discovery of reduced plasma physics models from fully kinetic simulations," in *APS Division of Plasma Physics Meeting Abstracts*, APS Meeting Abstracts, Vol. 2020 (2020) p. GO10.006.
- ⁶N. M. Mangan, S. L. Brunton, J. L. Proctor, and J. N. Kutz, "Inferring biological networks by sparse identification of nonlinear dynamics," *IEEE Transactions on Molecular, Biological and Multi-Scale Communications* **2**, 52–63 (2016).
- ⁷M. Hoffmann, C. Fröhner, and F. Noé, "Reactive sindy: Discovering governing reactions from concentration data," *The Journal of Chemical Physics* **150**, 025101 (2019).
- ⁸M. Sorokina, S. Sygletos, and S. Turitsyn, "Sparse identification for nonlinear optical communication systems: Sino method," *Opt. Express* **24**, 30433–30443 (2016).
- ⁹C. Fronk and L. Petzold, "Interpretable polynomial neural ordinary differential equations," *Chaos: An Interdisciplinary Journal of Nonlinear Science* **33**, 043101 (2023).
- ¹⁰R. T. Chen, Y. Rubanova, J. Bettencourt, and D. K. Duvenaud, "Neural ordinary differential equations," *Advances in neural information processing systems* **31** (2018).
- ¹¹Y. Rubanova, R. T. Q. Chen, and D. K. Duvenaud, "Latent ordinary differential equations for irregularly-sampled time series," in *Advances in Neural Information Processing Systems*, Vol. 32, edited by H. Wallach, H. Larochelle, A. Beygelzimer, F. d'Alché-Buc, E. Fox, and R. Garnett (Curran Associates, Inc., 2019).
- ¹²R. Dandekar, V. Dixit, M. Tarek, A. Garcia-Valadez, and C. Rackauckas, "Bayesian neural ordinary differential equations," *CoRR* **abs/2012.07244** (2020), 2012.07244.
- ¹³X. Li, T.-K. L. Wong, R. T. Q. Chen, and D. Duvenaud, "Scalable gradients for stochastic differential equations," in *Proceedings of the Twenty Third International Conference on Artificial Intelligence and Statistics*, Proceedings of Machine Learning Research, Vol. 108, edited by S. Chiappa and R. C. Landra (PMLR, 2020) pp. 3870–3882.
- ¹⁴P. Kidger, J. Morrill, J. Foster, and T. Lyons, "Neural controlled differential equations for irregular time series," *Advances in Neural Information Processing Systems* **33**, 6696–6707 (2020).

- ¹⁵P. Kidger, “On neural differential equations,” arXiv preprint arXiv:2202.02435 (2022).
- ¹⁶J. Morrill, C. Salvi, P. Kidger, and J. Foster, “Neural rough differential equations for long time series,” in *International Conference on Machine Learning* (PMLR, 2021) pp. 7829–7838.
- ¹⁷J. Jia and A. R. Benson, “Neural jump stochastic differential equations,” *Advances in Neural Information Processing Systems* **32** (2019).
- ¹⁸R. T. Chen, B. Amos, and M. Nickel, “Learning neural event functions for ordinary differential equations,” arXiv preprint arXiv:2011.03902 (2020).
- ¹⁹D. Duvenaud, M. Heinonen, M. Tiemann, and M. Welling, “Differential equations and continuous-time deep learning,” *Visualization and Decision Making Design Under Uncertainty*, 19 (2023).
- ²⁰C. Fronk, J. Yun, P. Singh, and L. Petzold, “Bayesian polynomial neural networks and polynomial neural ordinary differential equations,” (2023), arXiv:2308.10892 [cs.LG].
- ²¹S. Li, L. D. Xu, and S. Zhao, “The internet of things: a survey,” *Information systems frontiers* **17**, 243–259 (2015).
- ²²K. Rose, S. Eldridge, and L. Chapin, “The internet of things: An overview,” *The internet society (ISOC)* **80**, 1–50 (2015).
- ²³L. M. Mayr and D. Bojanic, “Novel trends in high-throughput screening,” *Current opinion in pharmacology* **9**, 580–588 (2009).
- ²⁴P. Szymański, M. Markowicz, and E. Mikiciuk-Olasik, “Adaptation of high-throughput screening in drug discovery—toxicological screening tests,” *International journal of molecular sciences* **13**, 427–452 (2011).
- ²⁵G. Balsamo, A. Agusti-Panareda, C. Albergel, G. Arduini, A. Beljaars, J. Bidlot, N. Bousserez, S. Boussetta, A. Brown, R. Buizza, C. Buontempo, F. Chevallier, M. Choulga, H. Cloke, M. Cronin, M. Dahoui, P. Rosnay, P. Dirmeyer, E. Dutra, and X. Zeng, “Satellite and in situ observations for advancing global earth surface modelling: A review,” *Remote Sensing* **10**, 2038 (2018).
- ²⁶H. Owadi, “Bayesian numerical homogenization,” *Multiscale Modeling & Simulation* **13**, 812–828 (2015).
- ²⁷M. Raissi and G. Karniadakis, “Hidden physics models: Machine learning of nonlinear partial differential equations,” *Journal of Computational Physics* **357** (2017), 10.1016/j.jcp.2017.11.039.
- ²⁸M. Raissi, P. Perdikaris, and G. E. Karniadakis, “Numerical gaussian processes for time-dependent and nonlinear partial differential equations,” *SIAM Journal on Scientific Computing* **40**, A172–A198 (2018).
- ²⁹M. Raissi, P. Perdikaris, and G. E. Karniadakis, “Physics informed deep learning (part ii): Data-driven discovery of nonlinear partial differential equations,” (2017), arXiv:1711.10566 [cs.AI].
- ³⁰M. Raissi, P. Perdikaris, and G. E. Karniadakis, “Physics-informed neural networks: A deep learning framework for solving forward and inverse problems involving nonlinear partial differential equations,” *Journal of Computational physics* **378**, 686–707 (2019).
- ³¹S. Cuomo, V. S. Di Cola, F. Giampaolo, G. Rozza, M. Raissi, and F. Piccialli, “Scientific machine learning through physics-informed neural networks: Where we are and what’s next,” *Journal of Scientific Computing* **92**, 88 (2022).
- ³²S. Cai, Z. Mao, Z. Wang, M. Yin, and G. E. Karniadakis, “Physics-informed neural networks (pinns) for fluid mechanics: A review,” *Acta Mechanica Sinica* **37**, 1727–1738 (2021).
- ³³G. G. Chrysos, S. Moschoglou, G. Bouritsas, J. Deng, Y. Panagakis, and S. Zafeiriou, “Deep polynomial neural networks,” *IEEE Transactions on Pattern Analysis and Machine Intelligence* **44**, 4021–4034 (2022).
- ³⁴S. Kim, P. Lu, S. Mukherjee, M. Gilbert, L. Jing, V. Ceperic, and M. Soljačić, “Integration of neural network-based symbolic regression in deep learning for scientific discovery,” *IEEE Transactions on Neural Networks and Learning Systems* **PP**, 1–12 (2020).
- ³⁵J. Kubalík, E. Derner, and R. Babuška, “Toward physically plausible data-driven models: A novel neural network approach to symbolic regression,” *IEEE Access* **11**, 61481–61501 (2023).
- ³⁶M. Zhang, S. Kim, P. Y. Lu, and M. Soljačić, “Deep learning and symbolic regression for discovering parametric equations,” (2023), arXiv:2207.00529 [cs.LG].
- ³⁷I. A. Abdellou and S. Mehrkanon, “Symbolic regression for scientific discovery: an application to wind speed forecasting,” in *2021 IEEE Symposium Series on Computational Intelligence (SSCI)* (2021) pp. 01–08.
- ³⁸X. Su, W. Ji, J. An, Z. Ren, S. Deng, and C. K. Law, “Kinetics parameter optimization via neural ordinary differential equations,” (2022), arXiv:2209.01862 [physics.chem-ph].
- ³⁹W. Ji and S. Deng, “Autonomous discovery of unknown reaction pathways from data by chemical reaction neural network,” *The Journal of Physical Chemistry A* **125**, 1082–1092 (2021).
- ⁴⁰N. Boddupalli, T. Matchen, and J. Moehlis, “Symbolic regression via neural networks,” *Chaos: An Interdisciplinary Journal of Nonlinear Science* **33**, 083150 (2023).
- ⁴¹S. Kim, W. Ji, S. Deng, Y. Ma, and C. Rackauckas, “Stiff neural ordinary differential equations,” *Chaos: An Interdisciplinary Journal of Nonlinear Science* **31**, 093122 (2021).
- ⁴²M. Caldana and J. S. Hesthaven, “Neural ordinary differential equations for model order reduction of stiff systems,” arXiv preprint arXiv:2408.06073 (2024).
- ⁴³H. E. Dikeman, H. Zhang, and S. Yang, “Stiffness-reduced neural ode models for data-driven reduced-order modeling of combustion chemical kinetics,” in *AIAA SCITECH 2022 Forum* (2022) p. 0226.
- ⁴⁴A. J. Linot, J. W. Burby, Q. Tang, P. Balaprakash, M. D. Graham, and R. Maulik, “Stabilized neural ordinary differential equations for long-time forecasting of dynamical systems,” *Journal of Computational Physics* **474**, 111838 (2023).
- ⁴⁵S. I. Holt, Z. Qian, and M. van der Schaar, “Neural laplace: Learning diverse classes of differential equations in the laplace domain,” in *International Conference on Machine Learning* (PMLR, 2022) pp. 8811–8832.
- ⁴⁶J. Baker, H. Xia, Y. Wang, E. Cherkaev, A. Narayan, L. Chen, J. Xin, A. L. Bertozzi, S. J. Osher, and B. Wang, “Proximal implicit ode solvers for accelerating learning neural odes,” arXiv preprint arXiv:2204.08621 (2022).
- ⁴⁷R. Malpica Galassi, P. P. Ciottoli, M. Valorani, and H. G. Im, “An adaptive time-integration scheme for stiff chemistry based on computational singular perturbation and artificial neural networks,” *Journal of Computational Physics* **451**, 110875 (2022).
- ⁴⁸T. Thummerer and L. Mikelsons, “Eigen-informed neural ordinary differential equations: Dealing with stability and convergence issues,” Available at SSRN 4819144.
- ⁴⁹Y. Weng, Z. Zhao, H. Zhang, and D. Zhou, “Extending fourier neural operators to learn stiff chemical kinetics,” in *40th International Symposium on Combustion (submitted)* (2024).
- ⁵⁰A. Ghosh, H. Behl, E. Dupont, P. Torr, and V. Nambodiri, “Steer: Simple temporal regularization for neural ode,” *Advances in Neural Information Processing Systems* **33**, 14831–14843 (2020).
- ⁵¹C. Finlay, J.-H. Jacobsen, L. Nurbekyan, and A. M. Oberman, “How to train your neural ode: the world of jacobian and kinetic regularization,” (2020), arXiv:2002.02798 [stat.ML].
- ⁵²J. Kelly, J. Bettencourt, M. J. Johnson, and D. Duvenaud, “Learning differential equations that are easy to solve,” (2020), arXiv:2007.04504 [cs.LG].
- ⁵³D. Onken and L. Ruthotto, “Discretize-optimize vs. optimize-discretize for time-series regression and continuous normalizing flows,” (2020), arXiv:2005.13420 [cs.LG].
- ⁵⁴D. Onken, S. W. Fung, X. Li, and L. Ruthotto, “Ot-flow: Fast and accurate continuous normalizing flows via optimal transport,” (2021), arXiv:2006.00104 [cs.LG].
- ⁵⁵S. Massaroli, M. Poli, M. Bin, J. Park, A. Yamashita, and H. Asama, “Stable neural flows,” (2020), arXiv:2003.08063 [cs.LG].
- ⁵⁶S. Massaroli, M. Poli, J. Park, A. Yamashita, and H. Asama, “Dissecting neural odes,” (2021), arXiv:2002.08071 [cs.LG].
- ⁵⁷W. Ji, W. Qiu, Z. Shi, S. Pan, and S. Deng, “Stiff-pinn: Physics-informed neural network for stiff chemical kinetics,” *The Journal of Physical Chemistry A* **125**, 8098–8106 (2021).
- ⁵⁸N. Guglielmi, A. De Marinis, A. Savastianov, and F. Tudisco, “Contractivity of neural odes: an eigenvalue optimization problem,” arXiv preprint arXiv:2402.13092 (2024).
- ⁵⁹A. Pal, Y. Ma, V. Shah, and C. V. Rackauckas, “Opening the blackbox: Accelerating neural differential equations by regularizing internal solver heuristics,” in *International Conference on Machine Learning* (PMLR, 2021) pp. 8325–8335.
- ⁶⁰A. Pal, A. Edelman, and C. Rackauckas, “Locally regularized neural differential equations: Some black boxes were meant to remain closed!” (2023), arXiv:2303.02262 [cs.LG].
- ⁶¹T. Kumara, A. Kumara, and P. Pala, “A physics-constrained neural ordinary differential equations approach for robust learning of stiff chemical kinetics,” arXiv preprint arXiv:2312.00038 (2023).

- ⁶²S. Massaroli, M. Poli, M. Bin, J. Park, A. Yamashita, and H. Asama, “Stable neural flows,” arXiv preprint arXiv:2003.08063 (2020).
- ⁶³S. J. Wright, “Numerical optimization,” (2006).
- ⁶⁴G. A. Bliss, “The use of adjoint systems in the problem of differential corrections for trajectories,” *JUS Artillery* **51**, 296–311 (1919).
- ⁶⁵A. Gholami, K. Keutzer, and G. Biros, “Anode: Unconditionally accurate memory-efficient gradients for neural odes,” arXiv preprint arXiv:1902.10298 (2019).
- ⁶⁶T. Pfaff, M. Fortunato, A. Sanchez-Gonzalez, and P. W. Battaglia, “Learning mesh-based simulation with graph networks,” (2021), arXiv:2010.03409 [cs.LG].
- ⁶⁷K. Hornik, M. B. Stinchcombe, and H. L. White, “Multilayer feedforward networks are universal approximators,” *Neural Networks* **2**, 359–366 (1989).
- ⁶⁸U. M. Ascher and L. R. Petzold, *Computer methods for ordinary differential equations and differential-algebraic equations*, Vol. 61 (Siam, 1998).
- ⁶⁹D. Griffiths and D. Higham, *Numerical Methods for Ordinary Differential Equations: Initial Value Problems*, Springer Undergraduate Mathematics Series (Springer London, 2010).
- ⁷⁰E. Hairer, S. Nørsett, and G. Wanner, *Solving Ordinary Differential Equations I: Nonstiff Problems*, Springer Series in Computational Mathematics (Springer Berlin Heidelberg, 2008).
- ⁷¹M. Soustelle, *An Introduction to Chemical Kinetics*, ISTE (Wiley, 2013).
- ⁷²J. Gutkind, *Signaling Networks and Cell Cycle Control: The Molecular Basis of Cancer and Other Diseases*, Cancer Drug Discovery and Development (Humana Press, 2000).
- ⁷³I. Peter, *Gene Regulatory Networks*, Current Topics in Developmental Biology (Elsevier Science, 2020).
- ⁷⁴P. Magal, P. Auger, S. Ruan, M. Ballyk, R. de la Parra, W. Fitzgibbon, S. Gourley, D. Jones, M. Langlais, R. Liu, et al., *Structured Population Models in Biology and Epidemiology*, Lecture Notes in Mathematics (Springer Berlin Heidelberg, 2008).
- ⁷⁵H. McCallum, *Population Parameters: Estimation for Ecological Models*, Ecological Methods and Concepts (Wiley, 2008).
- ⁷⁶F. Fan, J. Xiong, and G. Wang, “Universal approximation with quadratic deep networks,” *Neural Networks* **124**, 383–392 (2020).
- ⁷⁷R. Horn, R. Horn, and C. Johnson, *Topics in Matrix Analysis* (Cambridge University Press, 1994).
- ⁷⁸O. Axelsson, “A class of a-stable methods,” *BIT Numerical Mathematics* **9**, 185–199 (1969).
- ⁷⁹B. L. Ehle, *On Padé approximations to the exponential function and A-stable methods for the numerical solution of initial value problems*, Ph.D. thesis, University of Waterloo Waterloo, Ontario (1969).
- ⁸⁰E. Hairer and G. Wanner, “Stiff differential equations solved by radau methods,” *Journal of Computational and Applied Mathematics* **111**, 93–111 (1999).
- ⁸¹P. Virtanen, R. Gommers, T. E. Oliphant, M. Haberland, T. Reddy, D. Cournapeau, E. Burovski, P. Peterson, W. Weckesser, J. Bright, S. J. van der Walt, M. Brett, J. Wilson, K. J. Millman, N. Mayorov, A. R. J. Nelson, E. Jones, R. Kern, E. Larson, C. J. Carey, Í. Polat, Y. Feng, E. W. Moore, J. VanderPlas, D. Laxalde, J. Perktold, R. Cimrman, I. Henriksen, E. A. Quintero, C. R. Harris, A. M. Archibald, A. H. Ribeiro, F. Pedregosa, P. van Mulbregt, and SciPy 1.0 Contributors, “SciPy 1.0: Fundamental Algorithms for Scientific Computing in Python,” *Nature Methods* **17**, 261–272 (2020).
- ⁸²J. Bradbury, R. Frostig, P. Hawkins, M. J. Johnson, C. Leary, D. Maclaurin, G. Necula, A. Paszke, J. VanderPlas, S. Wanderman-Milne, and Q. Zhang, “JAX: composable transformations of Python+NumPy programs,” (2018).
- ⁸³I. Babuschkin, K. Baumli, A. Bell, S. Bhupatiraju, J. Bruce, P. Buchlovsky, D. Budden, T. Cai, A. Clark, I. Danihelka, A. Dedieu, C. Fantacci, J. Godwin, C. Jones, R. Hemsley, T. Hennigan, M. Hessel, S. Hou, S. Kapturowski, T. Keck, I. Kemaev, M. King, M. Kunesch, L. Martens, H. Merzic, V. Mikulik, T. Norman, G. Papamakarios, J. Quan, R. Ring, F. Ruiz, A. Sanchez, L. Sartran, R. Schneider, E. Sezener, S. Spencer, S. Srinivasan, M. Stanojević, W. Stokowiec, L. Wang, G. Zhou, and F. Viola, “The DeepMind JAX Ecosystem,” (2020).
- ⁸⁴E. Fehlberg, *Classical fifth-, sixth-, seventh-, and eighth-order Runge-Kutta formulas with stepsize control* (National Aeronautics and Space Administration, 1968).
- ⁸⁵E. Schäfer, “A new approach to explain the “high irradiance responses” of photomorphogenesis on the basis of phytochrome,” *Journal of Mathematical Biology* **2**, 41–56 (1975).
- ⁸⁶M. McKay, R. Beckman, and W. Conover, “A comparison of three methods for selecting values of input variables in the analysis of output from a computer code,” *Technometrics* **21**, 239–245 (1979).
- ⁸⁷V. Eglajs and P. Audze, “New approach to the design of multifactor experiments,” *Problems of Dynamics and Strengths* **35**, 104–107 (1977).
- ⁸⁸R. Iman, J. Helton, and J. Campbell, “An approach to sensitivity analysis of computer models, part 1. introduction, input variable selection and preliminary variable assessment,” *Journal of Quality Technology* **13**, 174–183 (1981).
- ⁸⁹R. Iman, J. Davenport, and D. Zeigler, “Latin hypercube sampling (program user’s guide),” Tech. Rep. OSTI 5571631 (Osti, 1980).